Doctoral Dissertation (Censored)

博士論文（要約）

Development of localized surface plasmon resonance sensors aiming for monitoring H_2S and SO_2 in volcanic gases

（火山ガスのH_2SとSO_2のモニタリングを目指した
局在表面プラズモン共鳴センサの開発）

A Dissertation Submitted for the Degree of Doctor of Philosophy
August 2021
令和3年8月博士（理学）申請

Department of Chemistry, Graduate School of Science,
The University of Tokyo
東京大学大学院理学系研究科　化学専攻

Yuki Takimoto
瀧本　悠貴

Abstract

1. Introduction

Volcanic gases are composed of H_2O, CO_2, SO_2, H_2S, HCl, HF, H_2, CO, S_2, N_2, CH_4, SiF_4 etc., and their chemical compositions and emission amount are important indicators of volcanic activity. In addition, volcanic gases are one of the major factors that cause volcanic disasters. Among volcanic gases, SO_2 and H_2S have been vigorously observed because they are highly toxic and are the most common volcanic gas species after H_2O and CO_2. Volcanic gases are conventionally observed by direct sampling and spectroscopic methods. Direct sampling methods allow for detailed analysis, but it is dangerous to directly collect gas samples from fumaroles. In addition, rapid assessment of volcanic activity is difficult because sample preparation and analysis in a laboratory are complex and time-consuming. Spectroscopic methods enable continuous measurement at a safe distance from active craters. However, they have limitations such as the need for an appropriate light source, the complexity of data analysis, the difficulty in autonomous operation, and the high cost of purchasing instrument. Recently, methods using small and low-cost electrochemical sensors have been developed for remote and real-time monitoring of volcanic gases. However, there are still some problems with the sensors, such as sensor stability, cross-sensitivities, uncertainties of gas ratios caused by differences in response time.

In recent years, localized surface plasmon resonance (LSPR) has been applied to sensing of various gases including H_2S, except for SO_2. LSPR is a phenomenon in which light induces collective vibration of electrons on a metal surface. LSPR sensing is conventionally carried out by measuring the peak shift of an LSPR absorption spectrum caused by refractive index change when target gas is flowed on metal nanostructures. In principle, LSPR sensors can respond quickly by change in refractive index and have robustness against corrosive gases using durable materials. By coating LSPR nanomaterials with appropriate adsorbents and applying chemical modification, high sensitivity and selectivity can be obtained, and multivariate analysis using multiple LSPR sensors makes it possible to distinguish multiple gases. Therefore, LSPR sensing can be a promising candidate for monitoring volcanic gases. In this study, I have developed LSPR chips for sensing H_2S and SO_2 by investigating chemical modification and adsorbents to enhance the sensitivity and selectivity.

2. Fabrication of LSPR chips

The finite-difference time-domain simulation revealed that the optimal diameter and pitch of a Au nanopattern for the gas detection were 400 nm and 800 nm, respectively. At first, the simulated Au nanopattern was fabricated using electron beam lithography (EBL) to confirm the agreement of its LSPR spectrum with the simulated one. The process of UV nanoimprint lithography (UV NIL) was established to produce LSPR chips more easily and quickly than EBL and thermal NIL. To improve an LSPR spectrum, the annealing temperature of Au nanopattern was optimized to 450 °C.

3. Mesoporous-silica-coated LSPR chips

The mesoporous silica layers on the Au-nanopatterned chips were modified with amine silane coupling reagents, 3-aminopropyltrimethoxysilane (APTMS) or (*N*,*N*-dimethylaminopropyl) trimethoxysilane (DAPTMS), by chemical vapor deposition. The amine-modified chips were able to detect 20 ppm of SO_2 in 10 min under a dry condition. The DAPTMS-modified chip showed the higher sensitivity than the APTMS-modified one and enabled to detect 0.6 ppm of SO_2. The enhancement of the sensitivities can be attributed to the high porosity and superficial hydroxyl groups of mesoporous silica, and the strong interaction between the amino or amine group and SO_2. On the other hand, the APTMS-modified chip showed the higher sensitivity to H_2S than the DAPTMS-modified one. The sensitivities of both chips to H_2S were lower than those to SO_2, indicating the selectivity to SO_2. Furthermore, the sensitivity to SO_2 was enhanced under a humid condition. However, the spectra greatly shifted with changes in relative humidity (RH) because H_2O is absorbed by the mesoporous silica layer. This result suggests that it is difficult to detect subtle changes in absorbance induced by the target gases without a water absorbent or dehumidifier.

4. ZnO-deposited LSPR chips

The Au-nanopatterned chips deposited with ZnO layer showed the high sensitivity and rapid response to H_2S and SO_2, enabling to detect 0.1 to 20 ppm of H_2S in 0.5 min at 70 % RH. The sensitivity to SO_2 was higher than that to H_2S. A correlation between the H_2S concentration and absorbance change was observed at 0.5 min after exposure to H_2S, but no correlation was observed above 0.5 min after exposure. As the thickness of ZnO

increased, the peak wavelength of LSPR upshifted and the peak width broadened. The sensitivity increased up to a ZnO thickness of 20 nm and remained almost constant in the range of 20–30 nm. Therefore, a ZnO thickness of 20–30 nm was sufficient to detect the target gas with high sensitivity. However, heating the ZnO-deposited chips in air could not regenerate the chips exposed to H_2S because of the grain growth of ZnO.

5. ZIF-8-coated LSPR chips

By coating ZIF-8 on a Au nanopattern as a benchmark metal organic framework (MOF), the sensitivity to SO_2 and H_2S increased with increasing RH, resulting in the detection of 0.1–10 ppm H_2S and 0.1–20 ppm SO_2 within 5 min at 70 % RH. The ZIF-8-coated chip was more sensitive to SO_2, while at 0 % RH it was less sensitive. Even higher concentrations of SO_2 would have been detected without the limitations of the gas generation system. By heating the chip coated with ZIF-8 at 200 °C in air, the sensitivity and LSPR spectrum could be regenerated about a dozen times. Moreover, the amount of humidity-induced shift in the LSPR spectra was much smaller than that of a DAPTMS-modified mesoporous-silica-coated chip. This will enable to measure the concentration of SO_2 and H_2S in volcanic gases without the use of a water absorbent or dehumidifier.

6. Conclusions

The LSPR chips coated with amine-modified mesoporous silica, ZnO, and ZIF-8 were developed for sensitive detection of SO_2 and H_2S from sub-ppm to ppm. In particular, the ZIF-8-coated chips demonstrated the high sensitivity, some selectivity and regeneration ability under high humidity, indicating the possibility of detecting typical concentrations of H_2S and SO_2 in volcanic gases. In practical, the developed chips can be used to measure integrated concentrations of H_2S and SO_2 for a certain period because the absorbance remained almost constant after the exposure to the gases was stopped. Furthermore, an observation system with multiple LSPR sensors coated with various adsorbents can be small, inexpensive and has the potential to measure all volcanic gas components. Thus, this study showed the future potential of LSPR sensing to measure volcanic gases.

Contents

Chapter 1. General introduction

1.1. Volcanic activity and gases

Volcanic gases are composed of H_2O, CO_2, SO_2, H_2S, HCl, HF, H_2, CO, S_2, N_2, CH_4, SiF_4 etc. and their chemical compositions and emission amount are important indicators of volcanic activity (Oppenheimer et. al., 1998; Shinohara, 2005a; Hirabayashi, 2015). In addition, volcanic gases are one of the major factors that cause volcanic disasters. An eruption occurs when volatile materials in the magma foam and rise because of a decrease in pressure in the magma or crystallization of the magma (Hirabayashi, 2015). In Japan, there are 111 active volcanoes, and many eruptions have occurred. The eruptions of Mt. Unzen in 1991 and Mt. Kiso Ontake in 2014 left 43 and 63 people dead or missing, respectively. In 2013, a new island was formed by an eruption near Nishinojima, located about 130 km west of Ogasawara Chichijima. In 2014, a phreatic explosion occurred at Kuchinoerabujima volcano. The mechanism of a phreatic explosion is that groundwater is vaporized at once by heat from the magma and high-temperature volcanic gases (Hirabayashi, 2015). In addition, volcanic gases contain toxic chemical components (Table 1.1), and poisoning accidents including death often occur. For example, 142 and 1746 people died by a large amount of CO_2 emission from Diëng volcanic complex in Indonesia in 1979 and Lake Nyos, a crater lake in Cameroon in 1986, respectively (Le Guern et. al., 1982; Kusakabe and Ohsumi, 1987). In Japan, since 1950, an average of one person per year has been killed by H_2S and SO_2 at about a dozen volcanoes such as Mt. Aso, Mt. Nasu, Mt. Tateyama (Hirabayashi, 2015). Therefore, the observation of volcanic gases is especially important for understanding the state of volcanic activity, eruption prediction and disaster prevention.

In many volcanoes around the world, changes in the amounts and ratios of HF, HCl, H_2S, SO_2, CO_2, H_2, and other emissions have been observed before eruptions (Hirabayashi, 1986). It is often observed that the emission of volcanic gases from a crater stops or becomes extremely low before an explosive eruption. This indicates that accumulation of volcanic gases in shallow areas just below the crater increases the pressure, triggering the explosive eruption (Hirabayashi, 2015).

Gas concentration ratio is a more stable indicator of volcanic activity than a single gas concentration, which strongly depends on the distance from the fumarole and the wind direction and speed (De Vito et. al., 2007). The main component of volcanic gases is water vapor, which accounts for more than 90%. The other components depend on various conditions such as location and temperature of gas plume, and subsurface magmatic and hydrothermal processes (Shinohara, 2005a; Hirabayashi, 2015). For example, volcanic gases with higher temperatures contain more HF, HCl, SO_2, H_2, and CO, while those with lower temperatures H_2S, CO_2, and N_2 as shown in Table 1.2 (Hirabayashi, 2015). The ratio of SO_2 and H_2S can change by the following reversible reaction:

$$SO_2 + 3H_2 \rightleftharpoons H_2S + 2H_2O$$

and this reaction proceeds to the left as the temperature rises or the pressure drops in the subsurface, increasing the SO_2/H_2S ratio (Hirabayashi, 1986; Oppenheimer et. al., 2011). Shinohara (2013) proposed that the gas supply mechanism of Mt. Shinmoedake is conduit magma convection based on the SO_2 fluxes and the gas compositions such as SO_2/H_2S and H_2O/CO_2. Aiuppa et. al. (2009) reported that the CO_2/SO_2 ratio of Stromboli plume is low in a relatively stable period (time-averaged ratio, 4.3) and high during the effusive phase (up to 21), particularly in the days and hours before a paroxysmal explosion. Thus, the concentration ratios of chemically related gas species can provide important information about volcanic activity.

As mentioned so far, SO_2 and H_2S are toxic gases and are important indicators of volcanic activity among volcanic gases. Therefore, they have been observed at many volcanoes, and various methods have been developed for the observation of SO_2 and H_2S, as described in the next section.

Table 1.1. Toxicity of volcanic gas components (Hirabayashi, 2015).

Gas composition	Concentration of smell	Lethal concentration	Permissible concentration
HF	?	600 ppm[*1]	3 ppm
HCl[*2]	1 ppm	1000 ppm	5 ppm
SO_2[*3]	0.3 - 1 ppm	500 ppm	2 ppm
H_2S	0.06 ppm	700 ppm	10 ppm
CO_2[*4]	Odorless	40 %	5000 ppm
CO[*5]	Odorless	1500 ppm	50 ppm

*1: Inhalation lethal concentration in guinea pigs. *2: Mucous membrane is irritated at 10 ppm. *3: Respiratory distress occurs at 30~40 ppm. *4: There have been cases of death in 5 minutes at 9 % and in 1 minute at 10 %. 10-15 % is said to cause coma in a few breaths. *5: A stay of 1 h in an environment of 1,500 ppm is life threatening.

Table 1.2. Chemical components and temperature of volcanic gases (volume %) (Hirabayashi, 2015).

Volcano	Temp.	H_2O	HF	HCl	SO_2	H_2S	CO_2	He	H_2	O_2	N_2	CO
Surtsey	1137	86.2		0.40	3.28		4.79		4.74	0	0.07	0.38
Unzen	810	97.2		0.196	0.498	0.196	1.28		0.586	0.079	0.148	0.1261
Satuma-Iwo	877	97.5	0.033	0.677	0.984		0.316	3E-6	0.474	5E-5	8.2E-3	1.1E-3
	740	97.8	0.048	0.00	0.975	0.075	0.561		0.396		0.035	
Kujyu	580	96.9		0.066	0.12	2.34	0.55					
	400	96.9	0.097	0.48	0.69	1.41	0.45		0.10		0.015	2.4E-4
	350	98.9	0.008	0.20	0.20	0.37	0.29	5E-6	3.1E-3		4.4E-3	
	185	99.2		0.0079	0.066	0.202	0.506		0.015		7.4E-3	2.3E-5
Nasu	530	98	0.014	0.06	0.178	0.712	0.952					
Kiso-Ontake	110	98.4		0.0003	0.018	0.323	1.254	4E-6	7.3E-4	1.8E-4	3.8E-3	
Kusatsu	95	97.8		0.0	0.2E-3	0.285	1.779	6E-6	2.1E-5		0.36	
Kirishima	98	97.4			3.4E-3	0.660	1.92	3E-6	1.4E-3	3.3E-4	0.018	

1.2. Conventional measurement methods of volcanic gases

Volcanic gases have been conventionally analyzed in a laboratory using gas chromatography, wet analysis and so on after direct sampling from fumaroles using evacuated bottles partially filled with alkaline solution. Figure 1.1 shows an example of

direct sampling, called Giggenbach bottle sampling (Giggenbach, 1975; Witt et. al., 2008). Gas samples are collected in an evacuated Pyrex flask with a NaOH aqueous solution through a titanium tube deeply inserted into a volcanic vent. Alkaline solution samples are analyzed for CO_2, total sulfur, HCI, HF and the average oxidation state of sulfur by chemical analysis such as titration. Non-absorbed gases, mainly H_2, CH_4, CO, N_2 and possibly O_2 are analyzed by gas chromatography. The direct sampling method can provide detailed analysis of volcanic gases, but it is dangerous, especially when volcanic activity becomes high, and the complex and time-consuming sample preparation and analysis in a laboratory mean that the analysis results are only available after several days. Thus, volcanic activity cannot be rapidly assessed in the field, and important changes in gas composition may not be found if the intervals between sample collections are long.

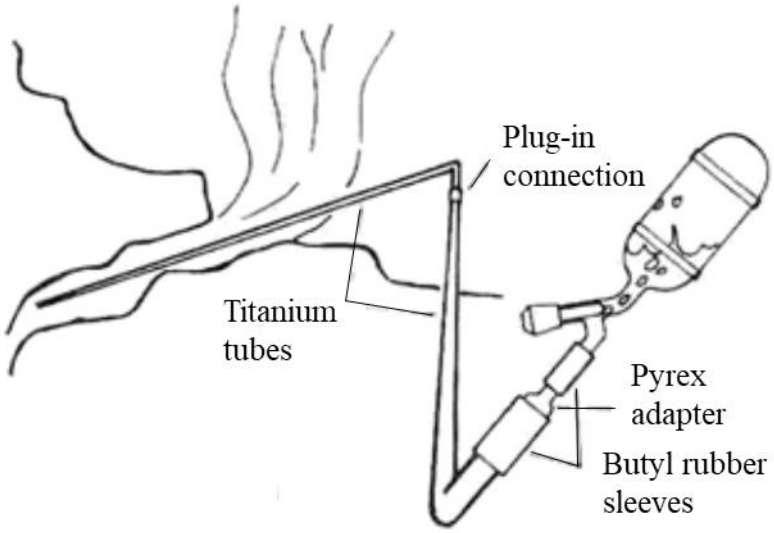

Figure 1.1. Direct gas sampling method using a Giggenbach bottle (Giggenbach, 1975).

Continuous measurement methods at a safe distance from active craters and fumaroles have been developed using Fourier transform infrared (FTIR) spectroscopy and ultraviolet (UV) spectroscopy, making it possible to evaluate volcanic activities and study the volcanic mechanism during eruptive periods.

The first FTIR spectroscopy of volcanic emissions of SO_2 was carried out in 1991 at Asama volcano, Japan (Notsu et. al., 1993). The significant advantage of FTIR method is

the ability to measure abundances of various volcanic gas species such as SO_2, HCl, HF, CO_2, CO, SiF_4, and OCS (Mori et. al., 1993; Francis et. al., 1996; Mori and Notsu, 1997; Oppenheimer et. al., 1998; Oppenheimer et. al., 2002; Mori and Notsu, 2008). Table 1.3 shows the typical concentrations and IR absorption bands of the major gases. However, the detection of H_2S in a volcanic plume is difficult because the bands are relatively weak and overlap with regions of stronger signals from H_2O and CO_2 (Oppenheimer et. al., 2011). H_2 and Cl_2 are also not detectable. Direct sunlight, fire fountains, lava lakes, hot rocks, and infrared lamps have been used as sources of infrared light, depending on the volcanic activity, access, and topography.

Table 1.3. Typical concentration ranges of major volcanic gas species in dilute plumes and their infrared absorption bands or lines (Oppenheimer et. al., 1998).

Gas species	Typical plume partial concentration (ppm)	Infrared absorption bands or lines (cm^{-1})
H_2O	10–1000	ubiquitous
CO_2	1–200	2050, 4850
SO_2	0.1–3	1100–1200; 1320–1400; 2450–2550
HCl	0.1–3	2700–2880
H_2S	0.1–0.5	1182, 2614, 2628
HF	< 1	4050–4150
CO	< 0.5	2146, 4230
SiF_4	< 0.005	1010–1040
OCS	0.005–0.1	2030–2090

The correlation spectrometer (COSPEC) is the first method to use UV spectroscopy for remote monitoring of SO_2 emitted from volcanic plumes and has been widely used since 1970s (Stoiber et al. 1973; Weibringa et. al., 2002). Since the introduction of low-cost and compact charge-coupled device (CCD) detectors in the early 2000s, differential optical absorption spectroscopy (DOAS) has been used instead of COSPEC (Mori et. al.,

2004). These methods use diffuse sky UV light as a light source to measure the absorption spectrum of SO_2 in a plume and to record the column density of SO_2. The amount of SO_2 in the plume cross section is observed from a fixed point, known as the panning method, or by passing under the plume while pointing a spectrometer's telescope upward from the ground with the spectrometer attached to a vehicle (car, ship, aircraft, etc.), known as the traverse method (Figure 1.2). The SO_2 flux can be estimated by multiplying the amount in the cross section and the plume velocity (Shinohara, 2005a; Oppenheimer et. al., 2011). The plume velocity may not represent the actual wind profile at the height and location of the plume because it must be estimated independently from hand-held devices or local weather stations. Therefore, the calculated SO_2 flux may have errors (Bluth et. al., 2007). In addition, there are some limitations in observation. For example, the method using the scattered sky light is restricted to daytime measurements and variations in plume flux occurring during the scan or faster than the sampling rate cannot be recognized. Furthermore, it is difficult to measure H_2S because of low UV radiation intensity of sky light at the required wavelengths (Roberts et. al., 2012).

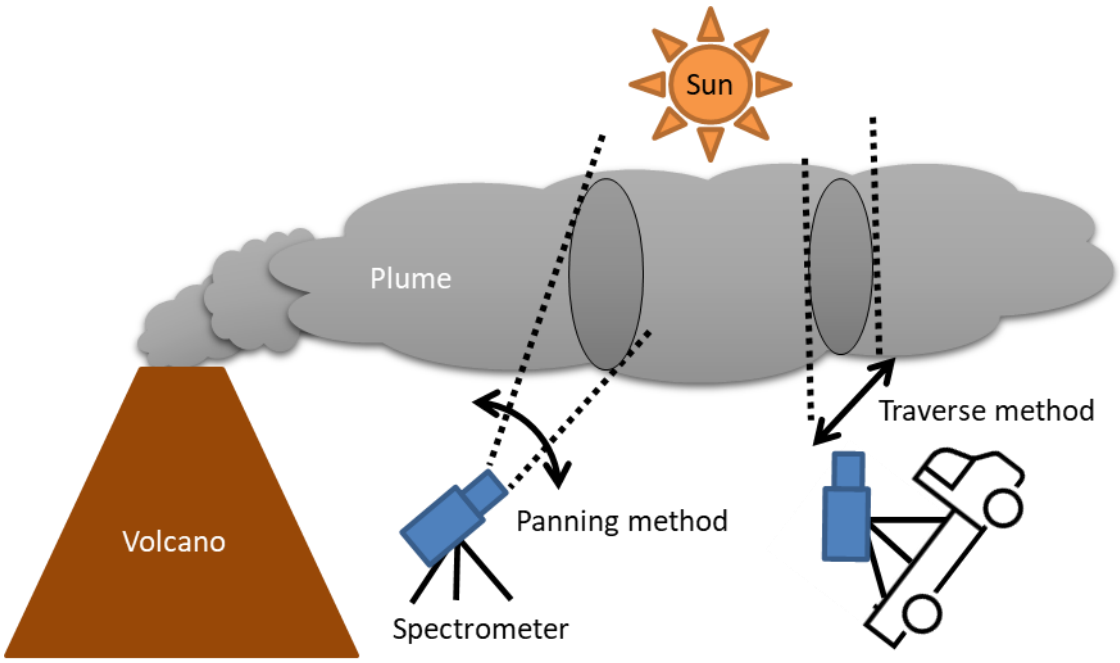

Figure 1.2. Schematic diagram of volcanic plume measurements by the panning and traverse methods.

Although these spectroscopic methods can detect a wide range of volcanic gases, they are not practical for real-time monitoring of active volcanoes on a global scale because of limitations, such as the requirement of an appropriate light source, complexity of data analysis, difficulty in autonomous operation, and the cost of purchasing instrument (Roberts et. al., 2012). Therefore, there is a growing interest in developing low-cost, low-power-consumption, portable instruments that can measure volcanic gases continuously (day and night), in real-time, and on the spot using electrochemical and spectroscopic sensors. The application of such in-situ sensors makes it possible to investigate spatial and temporal variations in the gas composition, compared to a time-averaged sampling or remote sensing methods that average over a path-length.

Shinohara (2005b) developed the first portable multi-sensor system, Multi-Gas, consisting of a humidity–temperature sensor, SO_2 electrochemical sensor, CO_2 IR analyzer, pump and flow control units, pressure sensor, data logger, and batteries. The whole system weighed only about 5 kg, which was light enough to be carried in a medium-size backpack. Shinohara (2005b) demonstrated that the composition of gas samples from Tokachi volcano estimated by this technique is consistent with the composition obtained by the conventional direct sampling method. At Stromboli volcano, changes in CO_2/SO_2 ratios have been observed for four times a day, every 30 minutes, for about four years using the Multi-Gas technique, and it may be possible to predict the recurrence of large explosions based on the release of CO_2-rich gas (Aiuppa et. al., 2011). Roberts et. al. (2012) developed a sensing system composed of six electrochemical sensors for SO_2, H_2S, CO, NO_2, and HCl (Figure 1.3a). Two CO sensors with low and high cross-sensitivities to H_2 were used. Near-simultaneous exposure and fast response are achieved by arranging the sensors in a parallel array (Figure 1.3b). The emissions from a fumarolic, crater lake and mixed plume of Aso volcano in Japan were measured at three locations around the crater rim by placing the system continuously for several hours for three consecutive days. The concentrations of SO_2, H_2S, CO, NO_2, and HCl were calculated from the current outputs of six sensors considering the cross-sensitivities, baseline drifts and the differences in response time. The H_2 concentration was also

obtained from the two CO sensors with the cross-sensitivities to H_2. Their concentrations typically ranged from about 0.1 to several tens of ppm, while NO_2 was not detected. Correction of uncertainties and bias in measured gas ratios (e.g. H_2S/SO_2) caused by the non-instantaneous response times of the sensors has been further investigated using mathematical models (Roberts et. al. 2014; Roberts et. al. 2017). In addition to calculation methods to correct the cross-sensitivity of a H_2S sensor to SO_2, an SO_2 scrubber was installed on the inlet of the H_2S sensor to prevent this cross-sensitivity (Shinohara et. al., 2011). Recently, remote sensing of SO_2 and H_2S was demonstrated using an unmanned aerial vehicle equipped with SO_2 and H_2S sensors with an SO_2 scrubber (Mori et. al., 2016).

Thus, low-cost, simple, and portable electrochemical sensors are expected to enable remote monitoring of volcanic gases at many volcanoes such as not only SO_2 but also H_2S and H_2, which are difficult to measure by spectroscopic methods. However, there are problems such as cross-sensitivities, uncertainties of gas ratios caused by different response times, baseline drifts and long-term stability. These problems have been tackled by various methods, but further improvements of sensors are required to obtain much more detailed data on volcanic activity.

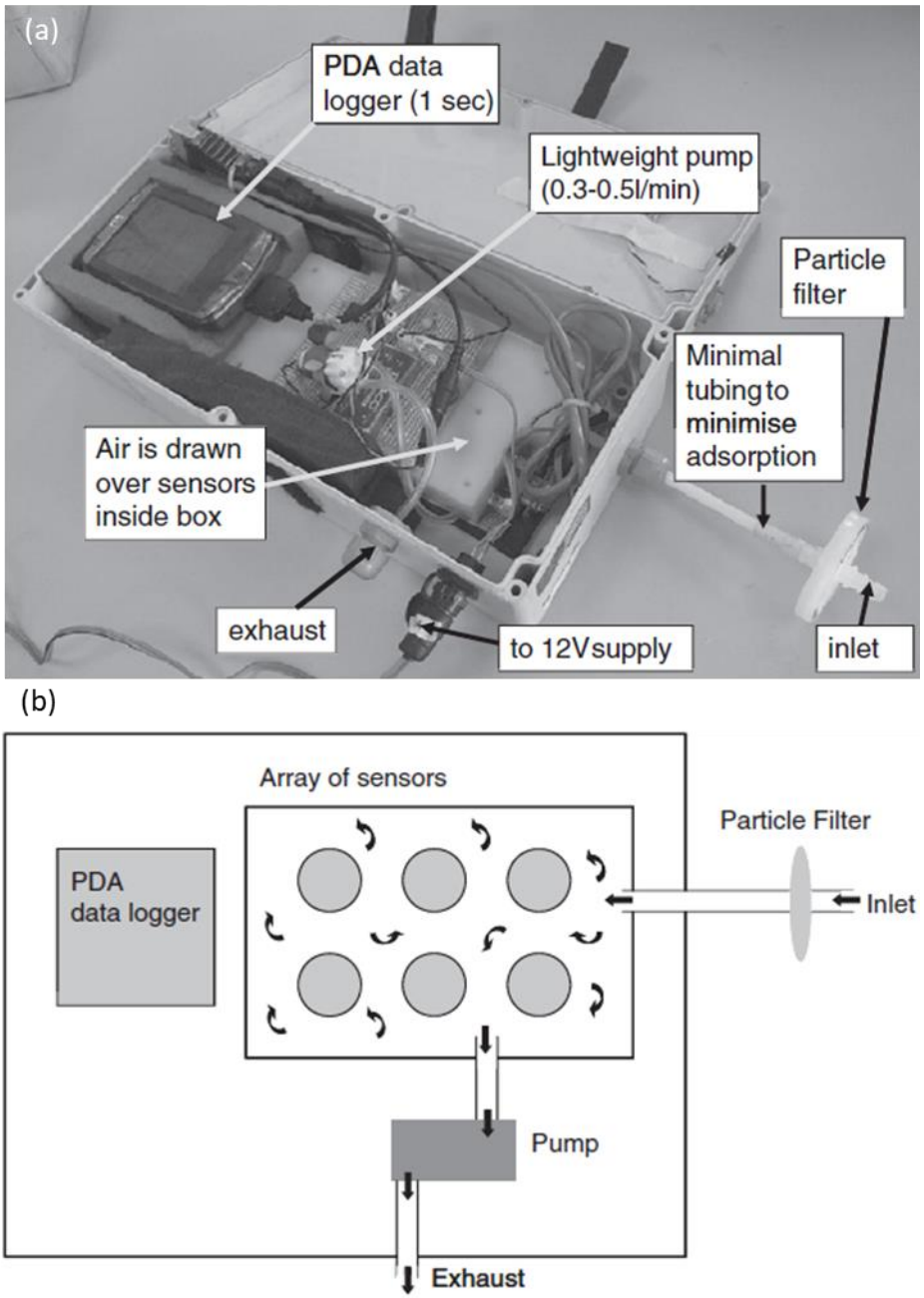

Figure 1.3. (a) Photograph of a portable instrument composed of six electrochemical sensors for detection of volcanic gases. The weight and size of the instrument are 2 kg and 36 cm × 16 cm × 10 cm, respectively. (b) Schematic diagram of a parallel sensor array design for near-simultaneous exposure to identical gas mixture (Roberts et. al., 2012).

1.3. Localized surface plasmon resonance

Localized surface plasmon resonance (LSPR) is a phenomenon that the electromagnetic field of light induces conduction electrons on a metallic nanostructure surface to vibrate collectively in resonance with a specific frequency of light, resulting in the absorption of a specific wavelength (Figure 1.4). The wavelength of the absorption spectrum, LSPR spectrum, depends on the metal species, its nanostructure, and the refractive index around the metal nanostructure.

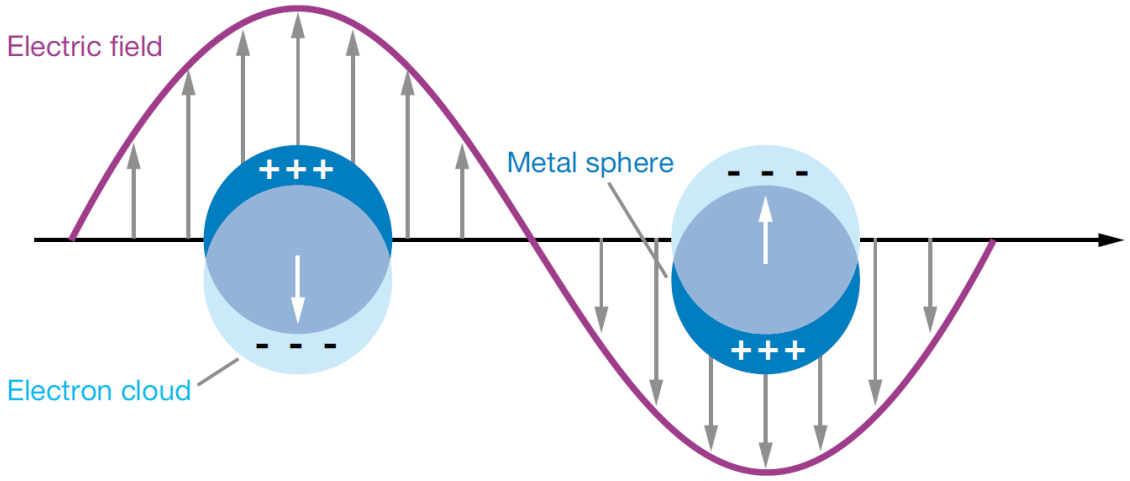

Figure 1.4. Schematic diagrams illustrating a localized surface plasmon (Willets et. al., 2007).

A theoretical treatment of LSPR is briefly explained using a spherical metal nanoparticle as the simplest model. According to the Mie solution of Maxwell's equation, when a spherical metal nanoparticle of radius a is irradiated with light of wavelength λ (a is much smaller than λ ($a/\lambda < 0.1$)), its extinction spectrum is calculated as follows:

$$E(\lambda) = \frac{24\pi^2 N a^3 \varepsilon_{out}^{\frac{3}{2}}}{\lambda \ln(10)} \left[\frac{\varepsilon_i(\lambda)}{(\varepsilon_r(\lambda)+\chi\varepsilon_{out})^2+\varepsilon_i(\lambda)^2} \right]$$

where ε_{out} is the dielectric constant of the external environment, ε_r and ε_i are the real and imaginary components of the metal dielectric function dependent on λ, respectively, and N is the number of spheres per unit volume (Willets et. al., 2007; Cao et al., 2014). The value of χ in front of ε_{out} is 2 for the case of a sphere and can only be solved analytically

for spheres and spheroids. Particles of arbitrary shape and size are analyzed by numerical methods such as the discrete dipole approximation (DDA) and the finite-difference time-domain (FDTD), which are the most popular methods (Draine and Flatau, 1994; Yurkin et. al., 2007; Oskooi et. al., 2010; Zhang et. al., 2011). An approximation to solve Maxwell's equations in the DDA and FDTD methods is to replace the target particle by a finite array of N-point dipoles and regular grids, Yee's mesh, respectively. The interaction of the dipoles with the applied electric field is evaluated in the frequency domain by the DDA. The electromagnetic field in Yee's mesh is solved in the time domain by the FDTD. The results simulated by both methods are usually in good agreement with the experimental results. The FDTD has a higher degree of freedom of shape and its calculation speed tends to be faster than the DDA when refractive index of a simulated model is 1.4 or higher. In this study, a Au nanopattern was optimized using FDTD simulation.

A change of refractive index (n) in the local medium surrounding the nanoparticles causes an immediate peak shift $\Delta\lambda$ of the LSPR spectrum. The shift expressed by the following equation is important for sensing applications (Willets et. al., 2007; Cao et al., 2014).

$$\Delta\lambda = m\Delta n\left[1 - \exp\left(\frac{-2d}{l_d}\right)\right]$$

Here m is the bulk refractive index response of the nanoparticles, Δn is the change in refractive index induced by adsorbates such as target molecules, d is the effective adsorbate layer thickness, and l_d is the characteristic electromagnetic-field-decay length. Refractive indices of gases such as volatile organic compound (VOC) and inorganic gases are closer to that of air than those of liquids (Table 1.4). This makes it difficult to detect low concentration of such gases in air because of an extremely small Δn. Therefore, to improve sensitivity or selectivity of LSPR sensors, metal nanostructures have been chemically modified or coated with gas adsorbents.

Table 1.4. Refractive indices of the gas or liquid materials.

Materials	State	Refractive index	Reference
Air	Gas	1.000292	1
N_2	Gas	1.000298	1
O_2	Gas	1.000271	1
Ar	Gas	1.000281	1
CO_2	Gas	1.000449	1
CO	Gas	1.000338	1
H_2	Gas	1.000132	1
He	Gas	1.000035	1
H_2S	Gas	1.000634	1
SO_2	Gas	1.000686	1
HCl	Gas	1.000447	1
H_2O	Gas (vapor)	1.000256	1
	Liquid	1.333	2
Ethanol	Gas	1.000878	1
	Liquid	1.3616	3
Acetone	Gas	1.001090	1
	Liquid	1.3591	3
Benzene	Gas	1.001762	1
	Liquid	1.4956	3
Toluene	Liquid	1.4966	3

*1: Kaye and Laby, Tables of Physical & Chemical Constants, National Physical Laboratory, https://web.archive.org/web/20190512005048/http://www.kayelaby.npl.co.uk/general_physics/2_5/2_5_7.html. Refractive index for the wavelength 589.3 nm (mean of sodium D lines) at a pressure of 101325 Pa and temperature of 0 °C, relative to a vacuum.

*2: Kaye & Laby Tables of Physical & Chemical Constants, National Physical Laboratory, https://web.archive.org/web/20190422005411/http://www.kayelaby.npl.co.uk/general_physics/2_5/2_5_8.html. Refractive index for the wavelength 589.3 nm (mean of sodium D lines) and

temperature of 20 °C or close to 20 °C.

*3: Mikhail Polyanskiy, Refractive index, https://refractiveindex.info. Accessed on 2021-06-04. Refractive index at 589.3 nm of benzene at 27 °C, and those of acetone, ethanol, and toluene at 20 °C.

Chen and Lu (2010) developed a sensor array consisting of three types of surface-modified metal nanomaterials that exhibit the LSPR absorbances at different wavelength regions in a UV-vis spectrum to detect nine VOC gases with various functional groups. The tested concentrations of the VOCs were, for example, 500–3000 ppm of 1-pentanol, 1000–3000 ppm of anisole, 4000–12000 ppm of toluene, 5000–25000 ppm of 2,2,2-trifluoroethanol and so on. Three types of the nanomaterials were decane-modified Ag nanoparticles, naphthalene-modified Au nanoparticles and 2-mercaptobenzothiazole-modified Au nano-shells. These chemical modifications gave some selectivity and different response patterns to VOC gases were obtained by simultaneously measuring the ensemble of the three LSPR spectra of the three nanomaterials. By cluster analysis of the response patterns, nine VOCs could be distinguished into three major groups. Low volatile compounds are easily absorbed and condensed on the surface of the nanomaterials, resulting in the calculated lowest detection limits (3σ) of 15–16 ppm for anisole and 1-pentanol, 128 ppm for toluene and 185 ppm for 2,2,2-trifluoroethanol. Moreover, the LSPR sensor coated with the mesoporous silica as a gas adsorption layer enabled to detect a wide range of concentrations of eighteen VOC gases from 10 to 1000 ppm (Monkawa et. al., 2014). In the case of toluene, concentrations from 1 to 20000 ppm were detected with a calculated detection limit of 0.40 ppm. The thermodynamically stable forms of the VOCs are liquids at room temperature and atmospheric pressure. Therefore, the sensitivity enhancement can be attributed to the capillary condensation of the VOC gases in porous silica which changes gases to liquids and increases their refractive indices. The large difference in the refractive indices between a liquid VOC and air causes a great peak shift in an LSPR spectrum, resulting in a significant increase in the sensitivity to the VOC gases. In addition, to enhance the sensitivity, they designed the Au nanopattern having the LSPR peak in the near-infrared region around 1250 nm

using FDTD simulation.

On the other hand, it is more difficult to detect low-concentration inorganic gases because they exist as gases and their capillary condensation cannot occur at room temperature and atmospheric pressure. Detection of inorganic gases with high concentrations in the order of % has been reported as follows. A low-noise LSPR spectrometer with high resolution using Ag and Au nanoparticles detected extremely small changes in the refractive indexes ($< 3 \times 10^{-4}$) between pure He (n = 1.000036) and Ar (n = 1.000281) or He and N_2 (n = 1.000298) (Bingham et. al., 2010). Kreno et. al. (2010) coated the Ag nanopattern with a metal organic framework (MOF) as an adsorbent, resulting in the detection of CO_2 concentration of ≥ 10%.

For detection of inorganic gases on the ppm order, it is necessary to investigate and improve metal nanomaterials, their pattern on a sensor substrate, their chemical modification, gas adsorbents, detection methods and so on. Joy et. al. (2012) developed a Au-CeO_2 nanocomposite film as a high-temperature LSPR gas sensor and detected H_2, CO, and NO_2 at 500 °C contained in three kinds of background gases: 5.0 % with a N_2 balance, 10 % O_2 with a N_2 balance and dry air (~21 % O_2). The observed change in the LSPR peak position was attributed to both changes in the dielectric surroundings and charge exchange with the Au nanoparticles induced by reduction of CeO_2 by H_2 and CO and oxidation by NO_2. This sensor could detect 100–10000 ppm of H_2, 200–2000 ppm of CO, and 2–98 ppm of NO_2, and make a distinction for separate gas exposures by analyzing the spectral information with the multivariate techniques. Cittadini et. al. (2014) deposited graphene oxide over a monolayer of Au nanoparticles and succeeded in the detection of 100 ppm H_2 and 1 ppm of NO_2 in air at 150 °C, while 10000 ppm of CO was not detected. The developed sensors have been tested several times for about 1 year, showing the reproducibility in LSPR peak shift and variation in absorbance.

While the detection of SO_2 using LSPR sensors has not been reported, there have been a few studies on the detection of H_2S. Au nanoparticles dispersed inside TiO_2-NiO thin films enabled to detect 2 ppm of H_2S at 350 °C and almost no interference was observed during simultaneous exposure to CO or H_2 (Della Gaspera et. al., 2010). The response to H_2S was found to be saturated in the concentration range of about 5–10 ppm.

The experimental evidence suggests that the direct catalytic oxidation of H_2S to SO_2 on the Au-TiO_2-NiO nanocomposite films is accompanied with a charge transfer between Au and S, which changes the LSPR spectra of Au nanoparticles. Chen et. al. (2013) reported that Ag nanoparticles were self-assembled to form a monolayer film on a glass substrate and detected 1–100 ppm of H_2S in N_2 at 25 °C by measuring the change in absorbance of the LSPR peak induced by the formation of Ag_2S. Because the change in absorbance was accumulated by exposure to H_2S, they expected that this sensor might be applied as a dosimeter, for example, to detect low H_2S concentrations that might pose risks to museums and library collections.

Although it is difficult to detect inorganic gases on the order of ppm with LSPR sensing, features such as robustness against corrosive gases, portability, low cost, good response, and wide dynamic range have been obtained by investigating plasmonic nanomaterials, gas adsorbents or chemical modification and so on. Moreover, multivariate analysis techniques using multiple LSPR sensors have demonstrated the possibility to overcome a lack of selectivity. Therefore, LSPR sensing can be a promising candidate for monitoring volcanic gases.

1.4. Purpose and contents of this study

Volcanic gases are one of the major factors that cause volcanic eruptions, and their chemical compositions and released amount are important information to understand volcanic activity and eruption mechanisms. In particular, SO_2 and H_2S have been vigorously observed because they are highly toxic and are the most common volcanic gas species after H_2O and CO_2. While observation of volcanic gases has been conventionally conducted by direct sampling and spectroscopic methods, methods using electrochemical sensors have also been developed. For example, by placing sensors around a crater rim, volcanic gases typically ranging from 0.1 to several tens of ppm were successfully detected. Since such sensors are small and low-cost, it is expected that they can be placed at many volcanoes to monitor volcanic activity remotely, safely, and in real time. However, there are still some problems with electrochemical sensors, such as sensor

stability, cross-sensitivities, uncertainties of gas ratios caused by difference in response times. Therefore, sensors which can overcome such problems are required. LSPR sensors are candidate for monitoring volcanic gases because in principle they can respond quickly by change in surrounding refractive index and have robustness against corrosive gases using durable materials such as Au nanoparticles on a SiO_2 substrate. High sensitivity and selectivity can be obtained by coating appropriate adsorbents and chemical modification on LSPR nanomaterials as well as multivariate analysis using multiple LSPR sensors which have different selectivities. In this study, H_2S and SO_2 sensors based on LSPR will be developed by investigating chemical modification and adsorbents to enhance the sensitivity and selectivity, demonstrating the detection of concentrations from 0.1 to 20 ppm (upper limit of a gas generation system in this study). This thesis consists of six chapters including introduction (Chapter 1) and conclusions (Chapter 6). In Chapter 2, the fabrication of LSPR sensor chips is described, and in Chapter 3–5, an amine-modified mesoporous silica, ZnO, and a metal organic framework were investigated as adsorbents of H_2S and SO_2.

Chapter 2. Fabrication of LSPR chips

本章については、5 年以内に雑誌等で刊行予定のため、非公開。

This chapter is not published because it is scheduled to be published in journals or other publications within five years.

Chapter 3. Mesoporous-silica-coated LSPR chips

3.1. Introduction

Low-cost and effective adsorbents based on mesoporous silica have been studied for the removal of harmful SO_2 gas before atmospheric emission in the power and chemical industries, as well as H_2S gas in natural gas, biogas, and crude oil (Rezaei et. al., 2015; Shah et. al., 2017; Khabazipour and Anbia, 2019). These gases can damage piping, facilities, and catalysts used in fuel cells or oil reformers. Mesoporous silica has pore sizes between 2.0 and 50 nm, high surface area, high porosity, narrow pore size distributions, good mechanical and thermal stability, and tunable structure (Khabazipour and Anbia, 2019). Mesoporous silica is typically synthesized by a sol-gel reaction (Alothman, 2012). A silica source such as tetraethyl orthosilicate (TEOS) and surfactant are mixed in an aqueous solution, and template of pore such as micelle is formed by self-assemble of surfactant, accompanied with the formation of silica gel. The gel is calcinated to remove the template of surfactant, resulting in mesoporous silica. Depending on synthesis conditions, mesoporous silica can have various structures, for example, hexagonal parallel packed nano-channels (known as MCM-41 and SBA-15), cubic 3D structures with interconnected short channels (MCM-48), and lamellar structures (MCM-50) (Khabazipour and Anbia, 2019). MCM-41 and SBA-15 have been extensively investigated because of their thermal, mechanical, and chemical resistance properties. Pore sizes of MCM-41 and SBA-15 are 1.5–10 nm and 4.6–30 nm, respectively, depending on the surfactants used as templates, the reaction parameters and so on (Zhao et, al., 1998; Alothman, 2012). However, the affinity of mesoporous silica toward H_2S and SO_2 is limited by its neutral framework. Therefore, amine groups which can strongly interact with H_2S and SO_2 have been modified on mesoporous silica surface to enhance their adsorption capacity (Rezaei et. al., 2015; Shah et. al., 2017; Khabazipour and Anbia, 2019).

One method of amine-modification is to immerse mesoporous silica in a solution containing amine molecules. Wang et. al. (2007) developed SBA-15 loaded with polyethyleneimine (PEI) by soaking SBA-15 in PEI solution and demonstrated that SBA-

15 adsorbed ppm level of H_2S in 20 % of H_2 balanced by N_2. The presence of moisture increased the adsorption capacity, while it reduced the desorption rate of the adsorbed H_2S. In addition, the developed adsorbent could be regenerated by purging pure N_2 at 100 °C overnight and showed stable sorption performance. SBA-15 loaded with triethanolamine by the soaking method showed the adsorption of SO_2 from a simulated flue gas composed of N_2, 11.04 % CO_2, and 1340 ppm SO_2, while the adsorption of CO_2 was negligible (Zhi et. al., 2011). The adsorbent was also resistant to moisture, had higher SO_2 capacity in the presence of moisture, and could be regenerated in N_2 stream at a rate of 100 mL/min for 30 min at 120 °C.

Amine-modification of mesoporous silica have been also carried out using amine-containing silane coupling reagents. For example, MCM-41 was modified with *N,N*-dimethylpropylamine or propyldiethanolamine by mixing the MCM-41 powder and the corresponding silane coupling reagents in toluene (Tailor et. al., 2014; Tailor and Sayari, 2016). The amine-modified MCM-41 showed the selective adsorption of SO_2 in the presence of CO_2 and higher SO_2 capacity in the presence of water vapor and could be regenerated at 130 °C under N_2.

Mesoporous silica has also been applied to LSPR sensing of biomolecules and chemical molecules. Coating of Au nanorods (NRs) with mesoporous silica shells stabilized the dispersion of Au NRs in various water−organic mixtures and pure organic solvents and succeeded in detecting glutathione (Wu and Xu, 2009). Moreover, Au NRs coated with mesoporous silica displayed higher sensitivity than non-coated Au NRs, and the further modification with specific antibody enabled the selective detection of the E. coli O157:H7 (Song et. al., 2017). A mesoporous silica containing Ag clusters detected nitroaromatic and nitroaliphatic explosives in solution with sensitivity down to concentrations of at least 1 μM (Zou et. al., 2012). Monkawa et. al. (2014) coated a Au nanopattern with a thin mesoporous silica layer and succeeded in the detection of eighteen VOC gases with high sensitivity and wide-dynamic-range. The enhancement in sensitivity is attributable to the capillary condensation of the VOC gases in mesoporous silica which increased their refractive indices.

This chapter describes Au nanopatterns coated with thin mesoporous silica layers

and further modified with amine groups for the enhancement of the adsorption capacity of H_2S and SO_2, leading to the high sensitivity.

3.2. Experimental procedures

3.2.1. Coating of mesoporous silica layer

A mesoporous silica layer was fabricated on a Au-nanopatterned chip by the sol-gel method following the procedure described in Monkawa et. al. (2014). Cetyltrimethylammonium bromide (CTAB) was dissolved in Milli-Q water at 60 °C and the pH of the solution was adjusted to 2.0 by adding HNO_3. Then, tetraethyl orthosilicate (TEOS) was slowly added and the solution was stirred for 3 h at room temperature. The final precursor solution with a molar ratio of CTAB:TEOS:H_2O = 1:8:185 was spin-coated on the Au-nanopatterned chip at 5000 rpm for 30 s. The substrate was then dried in an oven at 100 °C for 1 h. After drying, the template was removed by calcination in air at 450 °C for 1 h at a heating and cooling rate of 20 °C/min.

3.2.2. Modification of mesoporous silica layer with amine groups

A mesoporous silica layer was modified with 3-aminopropyltrimethoxysilane (APTMS) or (*N*,*N*-dimethylaminopropyl)trimethoxysilane (DAPTMS) by chemical vapor deposition as described in Hozumi et. al. (2001). A mesoporous-silica-coated chip was placed in a 100 mL Teflon container with a vial containing a mixture of 100 μL of APTMS or DAPTMS and 700 μL of toluene. The container was sealed with a cap and heated in an oven at 150 °C for 3 h. A chip modified with APTMS was sonicated for 20 min successively in ethanol, toluene, 1 mM NaOH, and 1 mM HNO_3. Finally, the chip was rinsed with Milli-Q water and then dried with N_2 gas. A chip modified with DAPTMS was sonicated for 20 min in ethanol, toluene and then dried with N_2 gas.

3.2.3. Characterization methods

Surface topographic images of the mesoporous-silica-coated chips were acquired with an atomic force microscope (AFM, SFT-3500; Shimadzu Corp., Japan). The thickness of the mesoporous silica layer was estimated from a cross section of the chip using a field-emission scanning electron microscope (FE-SEM, Quanta 3D FEG; FEI Company, USA). Depth profiles of atomic concentrations of C, N, O, Si, and Au were obtained by X-ray photoelectron spectroscopy (XPS, PHI Quantera IITM; Ulvac-Phi Inc., Japan) while etching with a 4 keV Ar ion beam for 30 s per XPS scan. The pass energy and X-ray source were 112 eV and Al Kα, respectively. The beam energy and diameter were 1486.6 eV and 100 μm, respectively.

3.2.4. Setup for gas measurements

A schematic diagram of the gas sensing system is shown in Figure 3.1a. Dry air (relative humidity (RH) < 1 %) generated by a clean air unit (P4-QD10; IAC Co., Ltd., Japan) was used as the background gas in the system. Dry air containing target gases such as SO_2 or H_2S was obtained from a standard gas generation system (Permeater PD-1B-2; Gastec Corp., Japan) using the permeation tube method. A three-way valve was used to switch between dry air containing the target gas and dry air without it. In this chapter, the gas flow rate was controlled to 500 mL/min by a mass flow controller (MQV 9500; Azbil Corp., Japan). An LSPR chip was placed in a chamber (28 mL in volume) (Figure 3.1b), which was respectively connected to the spectrometer and the light source through 400 μm diameter optical fibers. The light source was a tungsten halogen lamp (HL-2000; Ocean Optics Inc., USA. Size: 62 mm × 60 mm × 150 mm. Weight: 500 g. Power consumption: 7 W) optimized for the visible–NIR range (360–2500 nm). LSPR absorbance spectra were measured using a CCD-array NIR spectrometer (NIRQuest; Ocean Optics Inc., USA. Size: 182 mm × 110 mm × 47 mm. Weight: 1.18 kg. Power consumption: 15 W), of which the wavelength range and optical resolution were 900–1700 nm and 3.1 nm, respectively. All experiments were conducted at room temperature (25 °C).

The chamber containing the LSPR chip was placed in a gas corrosion test instrument (GH-180; Yamasaki Seiki kenkyusho Co., Ltd., Japan) to investigate the response of the LSPR chip to SO_2 gas under humid condition. The lid of the chamber was opened to expose the chip to the gas as shown in Figure 3.1b. The lamp and spectrometer were placed outside the instrument and connected to the chamber by the optical fibers.

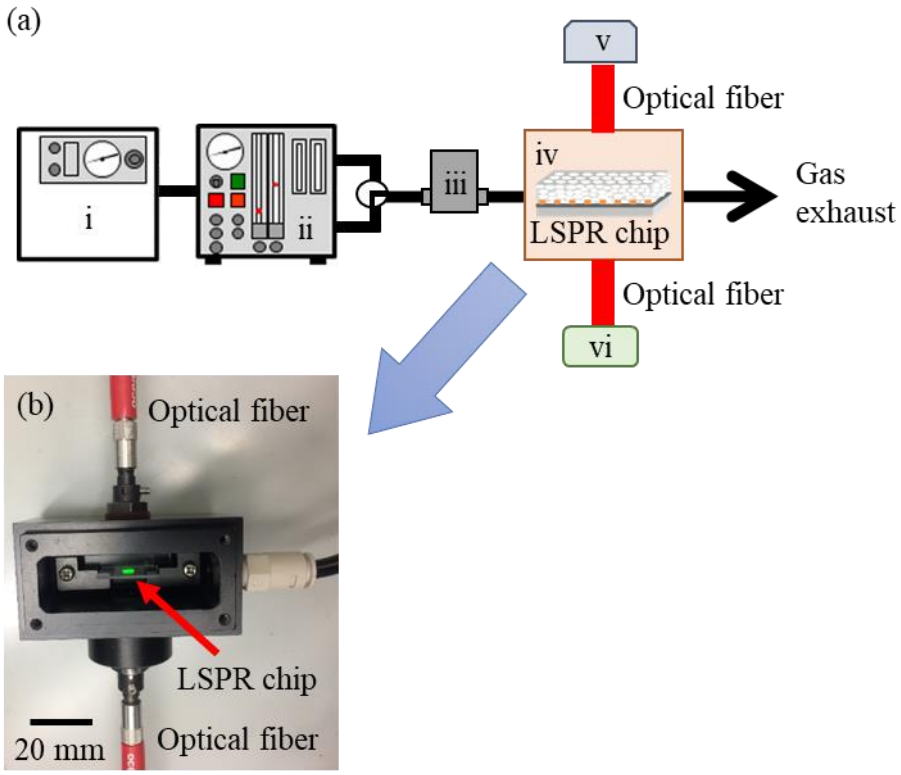

Figure 3.1. (a) Schematic diagram of the sensing system composed of a clean air unit (i), standard gas generation system (ii), mass flow controller (iii), chamber (iv), NIR spectrometer (v), and tungsten halogen lamp (vi). (b) Photograph of the chamber containing an LSPR chip.

3.3. Results and discussion

3.3.1. Coating of mesoporous silica layer on a Au-nanopatterned chip

Figure 3.2 shows the AFM image and cross-sectional SEM image of a Au-nanopatterned chip coated with a mesoporous silica layer of which the surface roughness

(Ra) was 7.8 nm. The thickness observed by FE-SEM was approximately 300 nm which was much higher than the height of the Au nanopattern (ca. 60 nm). These results indicate that the mesoporous silica layer covered the Au nanopattern completely and uniformly.

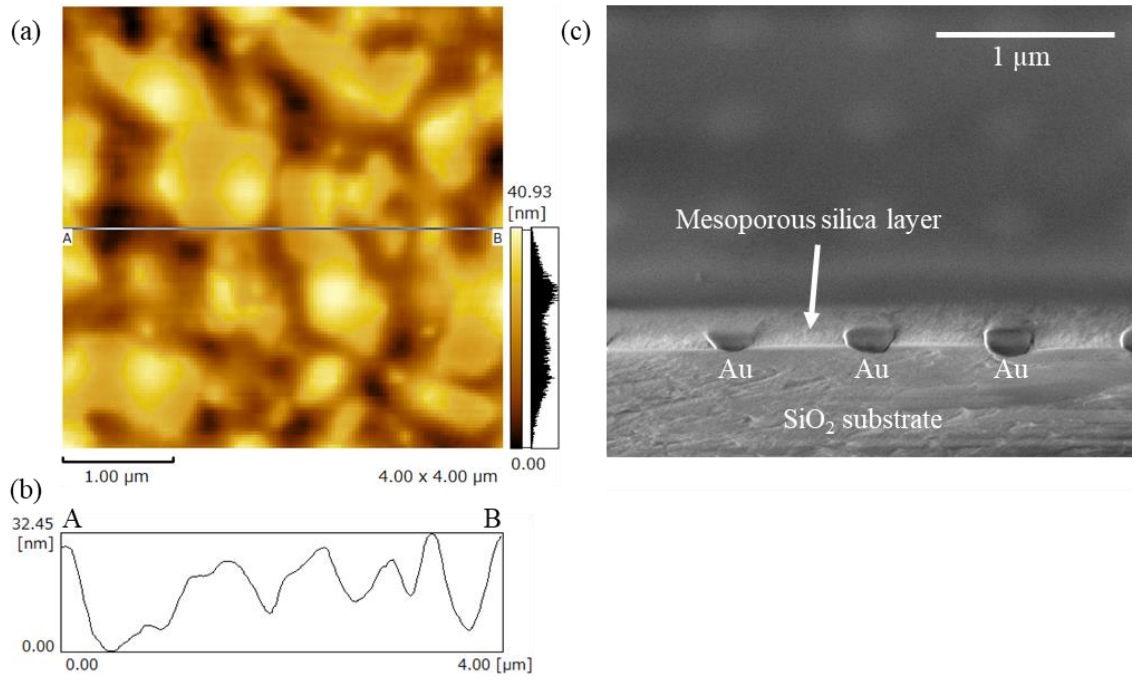

Figure 3.2. (a) AFM image, (b) profile, and (c) cross-sectional FE-SEM image of a mesoporous-silica-coated chip.

3.3.2. Modification of mesoporous silica layer with amine groups

Figure 3.3 shows the change in LSPR spectra by coating the mesoporous silica layer and modifying it with APTMS and DAPTMS. Coating the mesoporous silica layer narrowed the peak width of LSPR spectra and increased the absorbances. As mentioned in Chapter 2, these results are attributable to the annealing effect of Au, the oxidation of Si to SiO_2 and the formation of Au-Si eutectic. Furthermore, the modification with APTMS and DAPTMS shifted the peak wavelengths from 1224 to 1294 nm, and from 1185 to 1231 nm. The shifts induced by the CVD of APTMS and DAPTMS suggest that these silane coupling reagents were introduced into the mesoporous silica layers proximal

to the Au nanopatterns.

The depth profiles of the mesoporous-silica-coated, the APTMS-modified, and the DAPTMS-modified chip obtained by XPS measurements are shown in Figure 3.4. Whereas no C1s and N1s signals were detected in the mesoporous-silica-coated chip that was not modified with amine groups, these elements were present in the APTMS and DAPTMS-modified mesoporous-silica-coated chips. With increased etching time (depth), the concentrations of C1s and N1s became almost constant until the peak of Au4f appeared, indicating that both amine groups were modified by the mesoporous silica near the Au nanopattern. The atomic ratios of C1s/N1s were approximately three and five, which are consistent with the chemical formulae of the 3-aminopropyl group (C_3H_8N) of APTMS and the *N*,*N*-dimethylaminopropyl group ($C_5H_{12}N$) of DAPTMS, respectively. Three methoxy groups of both silane coupling agents were removed through a silane coupling reaction with mesoporous silica. The results obtained by the LSPR spectra and XPS measurements indicate that the mesoporous silica layer was uniformly modified with APTMS and DAPTMS.

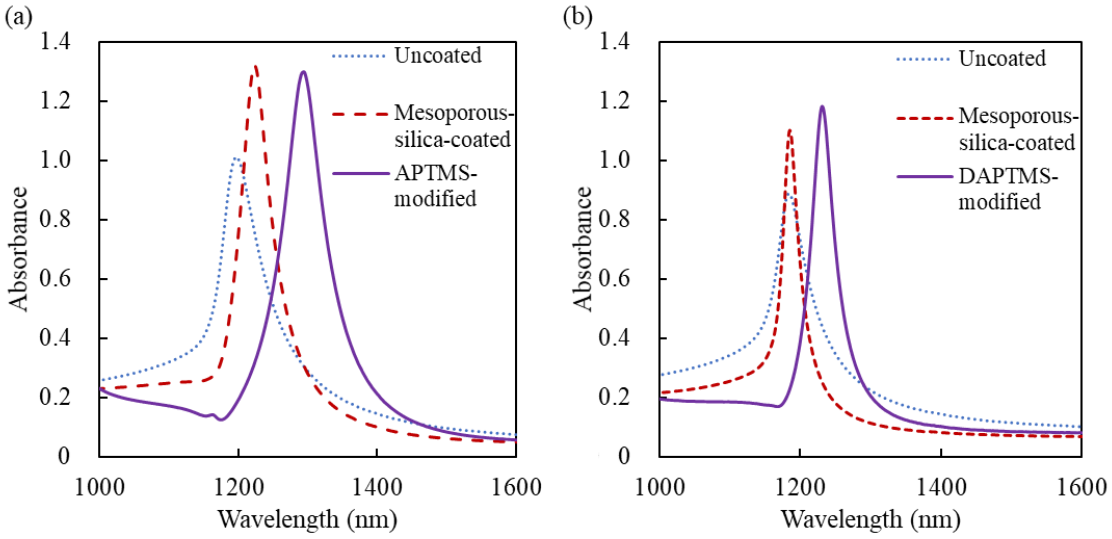

Figure 3.3. LSPR spectra of an uncoated Au-nanopatterned chip (blue dotted line), unmodified mesoporous-silica-coated chip (red dashed line), and amine-modified mesoporous-silica-coated chip (purple line). The modified amines were (a) APTMS and (b) DAPTMS.

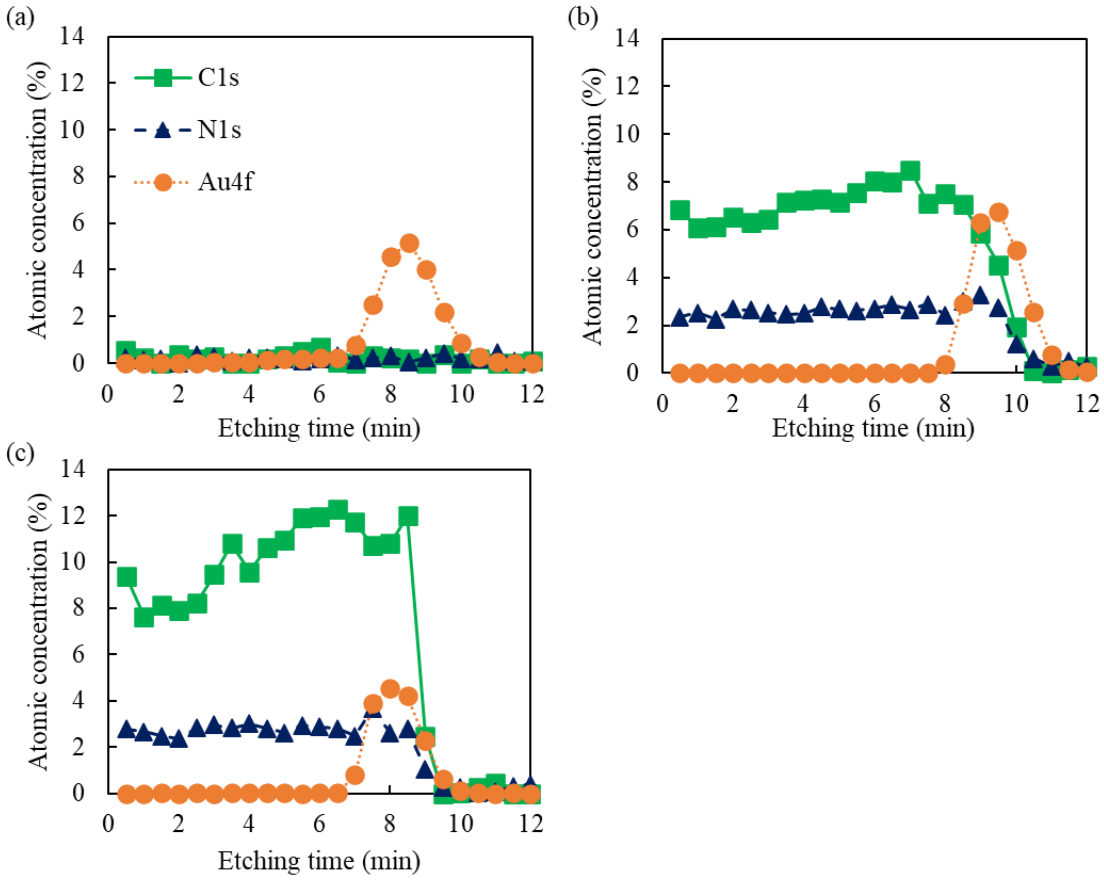

Figure 3.4. XPS depth profiles of an (a) unmodified, (b) APTMS-modified, and (c) DAPTMS-modified mesoporous-silica-coated chip. Note that the plots of O1s and Si2p derived from the mesoporous silica layers were removed from the figures.

3.3.3. Gas measurements

3.3.3.1. Measurement method for detecting the target gases

LSPR spectra shifted to higher wavelengths by exposure of LSPR chips to SO_2 gas. In the case of a DAPTMS-modified chip, the peak shift was approximately 1 nm in 10 min after the introduction of 20 ppm SO_2 gas (Figure 3.5). The amount is larger than the simulation result (0.06–0.07 nm shift induced by pure SO_2 as mentioned in section 2.3.1. in Chapter 2) because the mesoporous silica layer and amine-modification enhanced the sensitivity to SO_2 gas. Besides the peak shift, the subtle spectral changes can be detected

by observing the change in absorbance at a fixed wavelength. For example, by 20 ppm of SO_2 gas, the absorbance changed from 0.91 to 0.95 at 1232 nm (Figure 3.5b). This method is suitable for developing a portable and low-cost gas sensor because change in absorbance at a fixed wavelength can be measured by a photodiode and band-pass filter without a larger and more expensive spectrometer. In this study, absorbance change was observed at the higher wavelength of the inflection points of an LSPR spectrum before exposure to the target gases (SO_2 and/or H_2S). Inflection points were calculated by the differentiation of LSPR spectra as shown in Figure 3.5a.

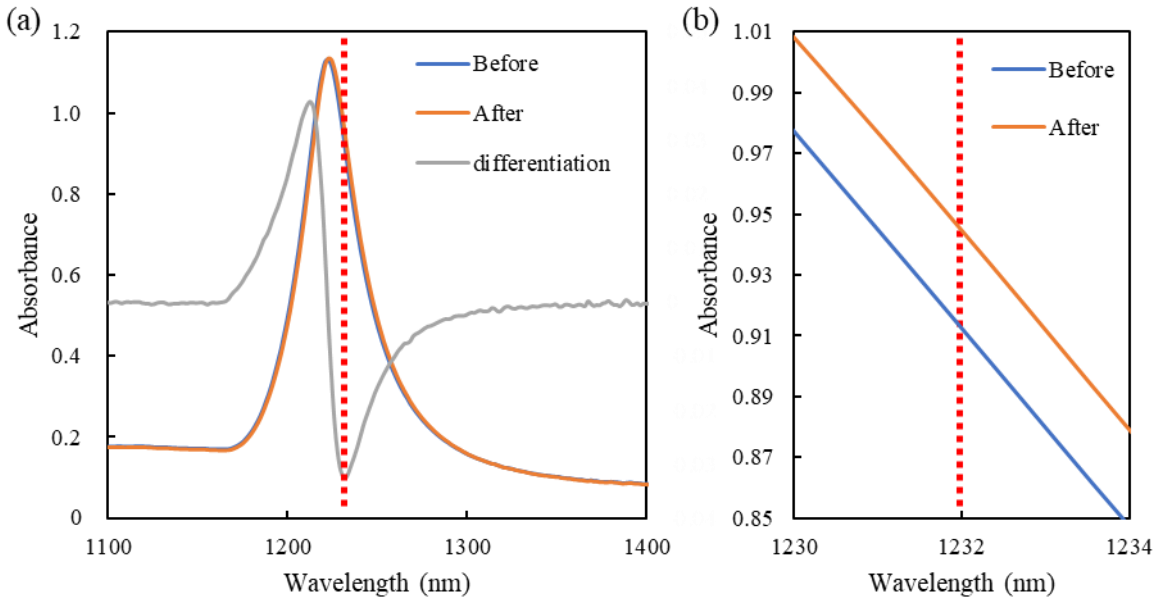

Figure 3.5. (a) LSPR spectra of the DAPTMS-modified chip before (blue line) and after (orange line) exposure to 20 ppm of SO_2 gas, and the differentiation curve of the spectrum before exposure (gray line). A red dashed line shows the position at 1232 nm. (b) Enlarged view of (a) from 1230 to 1234 nm.

3.3.3.2. Effect of amine-modification on the sensitivity to SO_2

Figure 3.6 shows the change in absorbance at 1200 nm for the uncoated Au-nanopatterned chip, 1191 nm for the mesoporous-silica-coated chip, 1237 nm for the APTMS-modified chip, and 1232 nm for the DAPTMS-modified chip during the SO_2

measurements under dry condition (< 1 % RH). Introduction of SO_2 gas resulted in the increase of absorbance at each wavelength of the inflection point. The change in absorbance of the mesoporous-silica-coated chip (0.52×10^{-3}) after 15 min corresponding to 10 min after the introduction of SO_2 gas was 2.6 times than that of the uncoated Au-nanopatterned chip (0.20×10^{-3}). Marcu et. al. (2004) proposed that sulfur dioxide adsorbs on zeolite by hydrogen bonding to one or two hydroxyl groups on the surface using the IR spectroscopy and the acidity measurement. Therefore, the improved sensitivity to SO_2 can be attributed to the coating of the Au nanopattern with the mesoporous silica layer which had the high porosity and surface hydroxyl groups.

Furthermore, the absorbance changes of the mesoporous-silica-coated chips modified with APTMS and DAPTMS (2.1×10^{-2} and 3.3×10^{-2}, respectively) were 40 and 63 times larger than that (0.52×10^{-3}) of the mesoporous-silica-coated chip, respectively. In the case of the DAPTMS-modified chips, 0.6 ppm of SO_2 could be detected (Figure 3.7). These drastic enhancement of the sensitivity to SO_2 possibly resulted from the strong interaction between the adsorbed SO_2 gas and amine groups as indicated in the following chemical reaction under dry condition (Tailor et. al., 2014):

$R_3N + SO_2 \leftrightharpoons R_3N \cdots SO_2$

Wong et. al. (1992) reported a theoretical study on charge-transfer (CT) molecular complexes between the methyl substituted amines and SO_2 using ab initio molecular orbital theory. The calculated enthalpies of complex formation and the amount of charge transfer from the amine to SO_2 were larger for $CH_3NH_2 \cdot SO_2$, $(CH_3)_2NH \cdot SO_2$, and $(CH_3)_3N \cdot SO_2$ in that order, which follows the donor strength of the amines (CH_3NH_2 < $(CH_3)_2NH$ < $(CH_3)_3N$). These results suggest that dimethyl amine group can interact with SO_2 more strongly than amino group, accounting for the higher sensitivity of the DAPTMS-modified chip than the APTMS-modified one.

After stopping the flow of SO_2 gas at 15 min, the absorbance gradually decreased in the case of both DAPTMS-modified and APTMS-modified chips (Figure 3.6). However, it did not return to the initial value of zero, suggesting that SO_2 did not desorb from the chips by the strong interaction with amine groups. Tailor et. al. (2014) developed *N*,*N*-dimethylpropylamine-grafted mesoporous silica as an adsorbent of SO_2. The adsorbent

saturated with SO_2 could be regenerated under both dry and humid conditions at 130 °C under N_2. However, the adsorbent could not be regenerated in humid condition (32 % RH) with O_2, resulting in the decrease of the adsorption capacity by 19.7 % compared to humid condition without O_2. In this study, the amine-modified chips could not be regenerated by heating (e.g., an APTMS-modified chip: 100 °C for 20 min in air, a DAPTMS-modified chip: 130°C for 2 h in air).

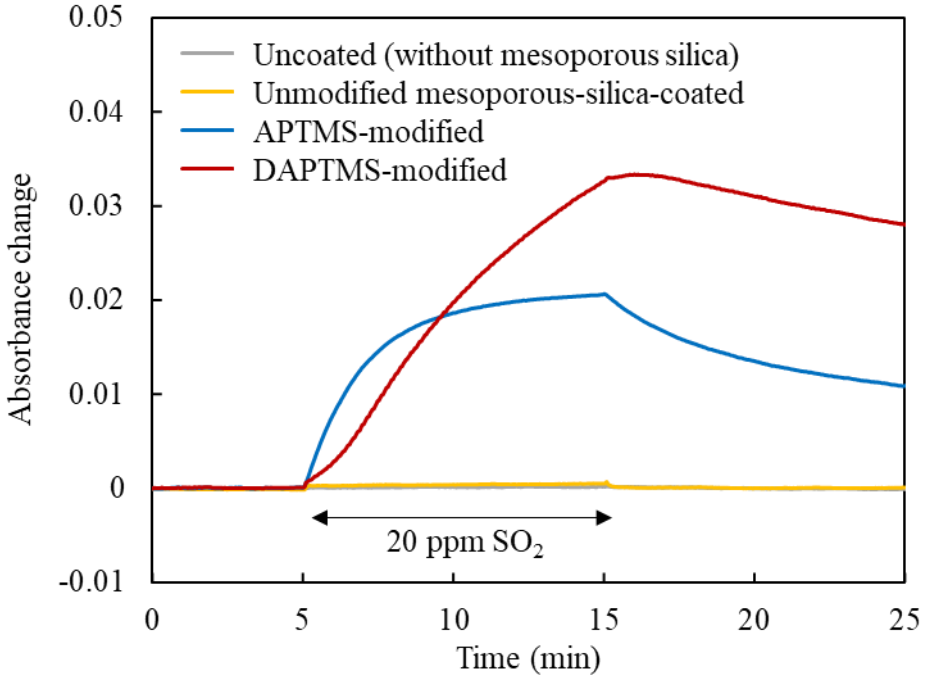

Figure 3.6. Response to 20 ppm SO_2 of an uncoated Au-nanopatterned chip at 1200 nm (gray line), mesoporous-silica-coated chip at 1191 nm (yellow line), APTMS-modified chip at 1237 nm (blue line) and DAPTMS-modified chip at 1232 nm (red line) under dry condition (< 1 % RH).

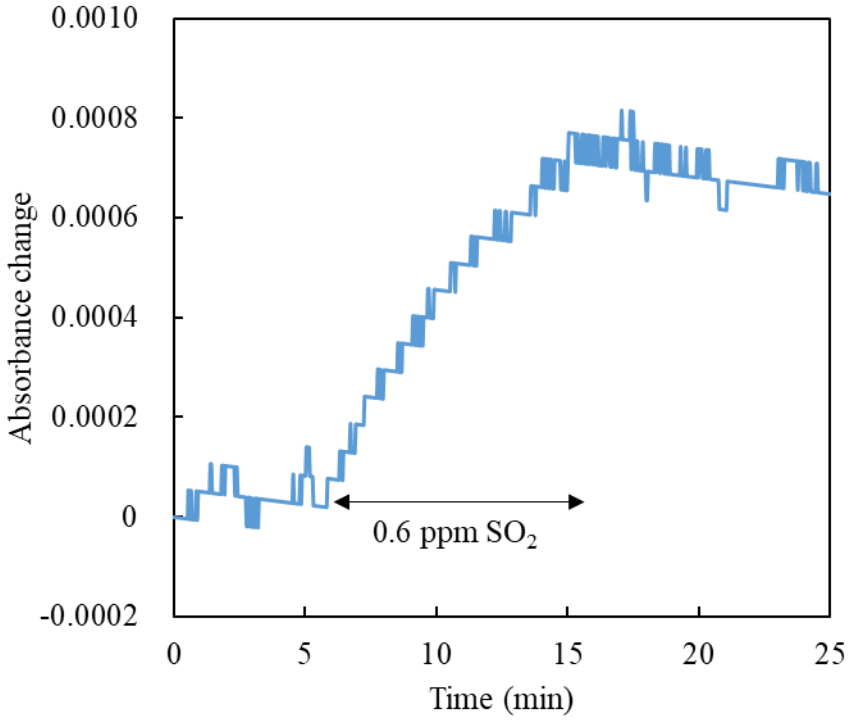

Figure 3.7. Response of a DAPTMS-modified chip to 0.6 ppm of SO_2 gas at 1258 nm. Note that this chip was different from the DAPTMS-modified chip in Figure 3.6.

3.3.3.3. Effect of amine-modification on the sensitivity to H_2S

The responses to H_2S gas were also examined under dry condition. The change in absorbance of the APTMS-modified mesoporous-silica-coated chip at 1237 nm was 3.5 × 10^{-3} 10 min after exposure to 20 ppm of H_2S, indicating the success in the detection of H_2S in ppm order (Figure 3.8). The absorption mechanism between H_2S and amine groups under dry condition is considered as follows (Wang et. al., 2007; Khabazipour and Anbia, 2019):

$H_2S + 2RNH_2 \rightleftharpoons RH_2NH—S—HNH_2R$

$H_2S + 2R_2NH \rightleftharpoons R_2HNH—S—HNHR_2$

$H_2S + 2R_3N \rightleftharpoons R_3NH—S—HNHR_3$

In these reactions, two amine groups interact with one molecule of H_2S. The other mechanism of H_2S-terriary amine reaction is also proposed as the following acid-base reaction (Shah et. al., 2017):

$H_2S + R_3N \rightleftharpoons R_3NH^+ + HS^-$

Although the amino group interacts with H_2S, the absorbance change induced by H_2S was 6 times smaller than that by SO_2 (2.1×10^{-2}), suggesting that the amino group preferred SO_2 to H_2S. It is also noteworthy that the absorbance did not decrease after stopping the flow of H_2S, while it decreased in the case of SO_2 gas. These results suggest that the SO_2 adsorption and desorption onto the amino group are kinetically more favorable, resulting in higher sensitivity and absorbance decrease after stopping the gas flow, or the adsorption of H_2S to the amino group is thermodynamically more favorable, resulting in no absorbance change after stopping the gas flow.

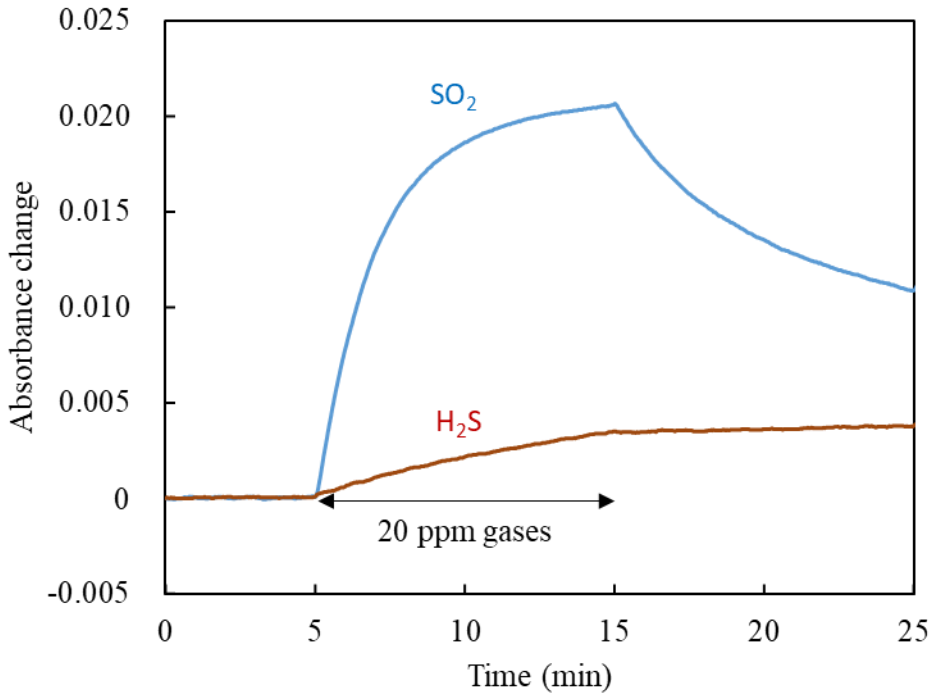

Figure 3.8. Responses of an APTMS-modified mesoporous-silica-coated chip to 20 ppm of SO_2 (blue line) and H_2S (red line) gas under dry condition.

In the case of the DAPTMS-modified mesoporous-silica-coated chip, the change in absorbance after exposure to 10 ppm of H_2S for 20 min was approximately 1.4×10^{-3}, which was 24 times smaller than the change in absorbance after exposure to 20 ppm of SO_2 for 10 min (3.3×10^{-2}), assuming that these total gas volumes were the same (Figure

3.9). This result indicates that the DAPTMS-modified chip was highly selective to SO_2.

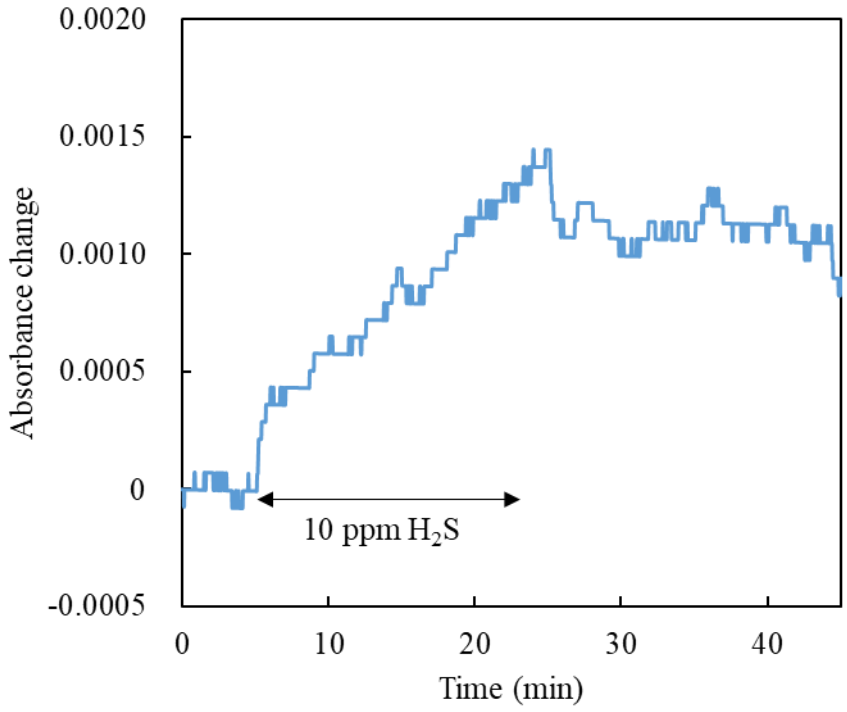

Figure 3.9. Response of a DAPTMS-modified mesoporous-silica-coated chip to 10 ppm of H_2S gas.

The absorbance change of the DAPTMS-modified chip (1.4×10^{-3} by 10 ppm H_2S for 20 min) was smaller than that of the APTMS-modified chip (3.5×10^{-3} by 20 ppm H_2S for 10 min) on the assumption that these total gas volumes were the same. This result can be attributed to steric hindrance of the higher number of methyl group substitutions. Okonkwo et. al. (2018) examined the H_2S absorption capacities of the mesoporous silicas (SBA-15) modified with APTMS, *N*-methylaminopropyltrimethoxysilane (MAPTMS), and DAPTMS using 1 or 10 % H_2S in N_2 at 30 °C. The absorption capacities were larger for DAPTMS, APTMS, and MAPTMS in that order. This trend was accordance with higher sensitivity to H_2S of the APTMS-modified chip than the DAPTMS-modified chip. The adsorption capacities of all the amine types gradually decreased in repeated exposure to H_2S (Okonkwo et. al., 2018). This reported result also suggests that it is difficult to use

repeatedly the amine-modified chips for detecting H_2S as well as SO_2.

3.3.3.4. Effect of relative humidity on the sensitivity

The response under humid condition was examined using a DAPTMS-modified chip, which had highest sensitivity and selectivity to SO_2 gas among the uncoated Au-nanopatterned, mesoporous-silica-coated, and APTMS-modified chip. As shown in Figure 3.10, the absorbance increased to ca. 8.0×10^{-2} after 10 min of exposure with 20 ppm of SO_2 gas at 95 % RH, which was 2.4 times larger than that in the case of dry condition (< 1 % RH), and reached a plateau at 9.7×10^{-2}. This enhancement can be attributable to the salt-forming reaction between amine group and SO_2 in the presence of H_2O as follows (Tailor et. al., 2014):

$R_3N + H_2O + SO_2 \leftrightarrows R_3NH^+HSO_3^-$

The sensitivity enhancement under humid condition is generally useful to monitor SO_2 gas under atmospheric conditions in natural environment containing H_2O.

In addition, the LPSR spectrum shifted to higher wavelength with increase of RH, indicating that H_2O molecules were absorbed in the mesoporous silica layer (Figure 3.11). For example, the wavelengths of the inflection points of the spectra at < 1, 74, and 95 % RH were 1258, 1280, and 1286 nm, respectively. However, large spectral shifts induced by RH changes make it difficult to detect small absorbance changes by low concentrations of SO_2 at a fixed wavelength such as 1286 nm. It is also not appropriate to observe absorbance changes at a single wavelength because the inflection points of the spectra vary greatly with humidity changes. Thus, in practical situation such as measurement of volcanic gases, a measurement system which can reduce humidity before gas exposure to a sensor is necessary in addition to the development of LSPR sensors that are not much affected by humidity.

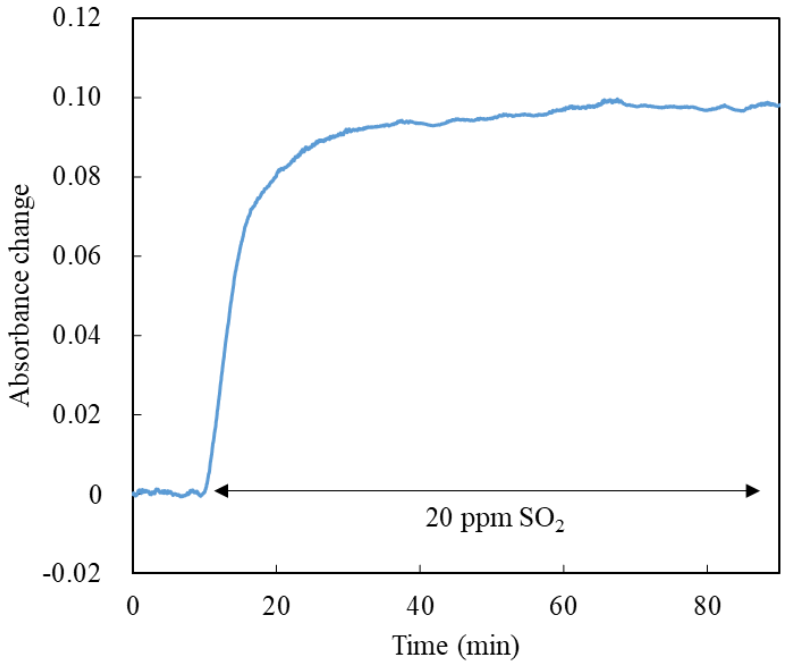

Figure 3.10. Response to 20 ppm of SO_2 at 95 % RH using a DAPTMS-modified chip measured at 1286 nm.

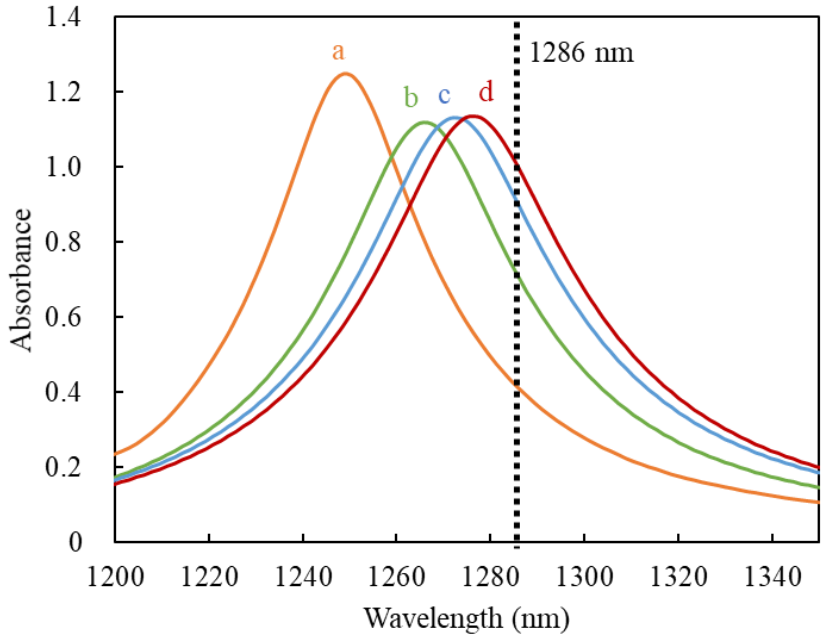

Figure 3.11. LSPR spectra of a DAPTMS-modified chip at (a) < 1, (b) 74, (c) 95 % RH, and (d) 95 % RH after exposure to 20 ppm of SO_2 gas. A black dashed line shows the position at 1286 nm, which is the inflection point of (c) the LSPR spectrum at 95 % RH.

3.4. Conclusions

The Au-nanopatterned chips were coated with mesoporous silica layers and modified with APTMS or DAPTMS by CVD, resulting in the detection of SO_2 and H_2S at ppm levels. The mesoporous silica coating enhanced the sensitivity to SO_2 gas because of the high porosity and superficial hydroxyl groups of mesoporous silica. Furthermore, the modification of the mesoporous silica layers with APTMS or DAPTMS drastically enhanced the sensitivity to SO_2 gas because of the strong interaction between the amino or amine group and SO_2. The DAPTMS-modified chip was able to detect 0.6 ppm of SO_2. The sensitivity of the DAPTMS-modified chip was higher than that of the APTMS-modified chip. Conversely, the APTMS-modified chip was more sensitive to H_2S although the sensitivities of both chips to H_2S were lower than those to SO_2. Thus, the amine-modified mesoporous-silica-coated chips enable the detection with high selectivity and sensitivity. In the case of the APTMS-modified chip, the absorbance remained constant even after the exposure to H_2S was stopped. Therefore, the APTMS-modified chip can be used to measure the integrated concentration of H_2S. On the other hand, for both chips, it is difficult to measure the accumulated concentration of SO_2 because the absorbances decreased to some extent after the exposure to SO_2 was stopped. Additionally, the sensitivity to SO_2 was enhanced under humid condition. This may be attributed to the strong salt formation among the amine group, SO_2 and H_2O. However, the spectra were greatly shifted by RH changes because of H_2O absorption in mesoporous silica layer, resulting in large differences of the inflection points. This feature makes it difficult to detect subtle absorbance changes induced by the target gases at a fixed wavelength. In practical use in the measurement of volcanic gases, it is necessary to investigate adsorbents that are not much affected by humidity or to place a water absorbent or dehumidifier on the inlet of a sensor system.

Chapter 4. ZnO-deposited LSPR chips

本章については、5 年以内に雑誌等で刊行予定のため、非公開。

This chapter is not published because it is scheduled to be published in journals or other publications within five years.

Chapter 5. ZIF-8-coated LSPR chips

本章については、5 年以内に雑誌等で刊行予定のため、非公開。

This chapter is not published because it is scheduled to be published in journals or other publications within five years.

Chapter 6. Conclusions

LSPR chips of Au nanopatterns coated with amine-modified mesoporous silica, ZnO, and ZIF-8 were fabricated and succeeded in the highly sensitive detection of SO_2 and H_2S at sub-ppm to ppm order. This is the first study of the detection of SO_2 based on LSPR as well as H_2S using the LSPR substrates coated with these adsorbents.

By FDTD simulation, the diameter and pitch of a Au nanopattern for the gas detection were optimized to be 400 nm and 800 nm, respectively. The simulated Au nanopattern was fabricated using EBL at first, revealing that the LSPR spectrum almost agreed with the simulated one. The process of UV NIL was established to produce LSPR chips more easily and quickly than EBL and thermal NIL. The Au nanopatterns fabricated by UV NIL also had the desired morphology and LSPR spectra. The annealing of the nanopattern at 450 °C narrowed the LSPR peak width and shifted the peak wavelength to the lower wavelength probably because of the grain growth of Au, the oxidation of the thin Si layer to SiO_2 and/or the formation of Au-Si eutectic.

The modification of the mesoporous silica layers on the Au-nanopatterned chips with the amine silane coupling reagents, APTMS or DAPTMS, enhanced the sensitivities to SO_2, demonstrating the detection of 20 ppm SO_2 in 10 min under dry condition. The DAPTMS-modified chip showed the higher sensitivity than the APTMS-modified one and enabled to detect 0.6 ppm SO_2. The enhancement of the sensitivities can be attributed to the high porosity and superficial hydroxyl groups of mesoporous silica, and the strong interaction between the amino or amine group and SO_2. On the other hand, the APTMS-modified chip showed the higher sensitivity to H_2S than the DAPTMS-modified one. The sensitivities of both chips to H_2S were lower than those to SO_2, indicating the selectivity to SO_2. In the case of the APTMS-modified chip, the absorbance remained constant after stopping exposure to H_2S. Therefore, the APTMS-modified chip can be used to measure a total or average concentration of H_2S for a certain period of time, e.g. 10 min. On the other hand, the absorbances of both chips decreased to some extent after stopping exposure to SO_2, making it difficult to measure integrated concentration of SO_2. Because of the different responses to H_2S and SO_2, it is difficult to calculate their concentrations

in the gas mixture by data analysis. The spectra shifted greatly with RH because of the absorption of H_2O in the mesoporous silica layer, although the sensitivity to SO_2 increased with humidity. This feature makes it difficult to detect subtle absorbance changes induced by the target gases at a fixed wavelength. Therefore, for practical use in the measurement of volcanic gases, it is necessary to place a water absorbent or dehumidifier at the inlet of a sensor system.

The deposition of ZnO layer on the Au-nanopatterned chips also increased the sensitivity to H_2S and SO_2 and shortened the response time, enabling to detect 0.1 to 20 ppm of H_2S in 0.5 min at 70 % RH. Thus, the ZnO-deposited chips were able to detect the low concentration range with the almost same time as electrochemical sensors. The sensitivity to SO_2 was higher than that to H_2S. A correlation between the H_2S concentrations and absorbance changes was observed at 0.5 min after exposure to H_2S, but no correlation was observed above 0.5 min after exposure, suggesting that it is difficult to measure highly concentrated gases. Unlike the amine-modified mesoporous-silica-coated chips, the absorbances remained almost constant even after H_2S and SO_2 were stopped. Therefore, the ZnO-deposited chips can be applied to measure integrated concentrations for 0.5 min. However, their low selectivity will limit the measurement target to either H_2S or SO_2. As the thickness of ZnO was increased, the peak wavelength of LSPR peak shifted to higher and the peak width broadened, and the sensitivity was enhanced up to 20 nm. The sensitivity was almost constant in the range of 20–30 nm thickness. These results indicate that a ZnO thickness of 20–30 nm was sufficient for sensitive detection of the target gas. However, heating the ZnO-deposited chips in air could not regenerate the chips after exposures to H_2S because the growth of ZnO grains on the surface caused the sensitivity to be unstable. Since the chips can be made small and inexpensive, it may be possible for practical use to store many chips in an observation system and automatically dispose of them in order to observe H_2S or SO_2 in volcanic gases regularly.

The sensitivity to SO_2 and H_2S was enhanced by coating of ZIF-8 as a benchmark MOF on a Au nanopattern and increased with RH. At 70 % RH, the ZIF-8-coated chip enabled to detect 0.1–10 ppm H_2S and 0.1–20 ppm SO_2 within 5 min and was more

sensitive to SO_2, while at 0 % RH it was less sensitive. Even higher concentrations of SO_2 would have been detected without the limitations of the gas generation system, indicating the potential of detecting typical concentrations of SO_2 in volcanic gases. Similar to the ZnO-deposited chips, the absorbances remained almost constant after stopping H_2S and SO_2, and the integrated concentration can be measured within 5 min for the ZIF-8-coated chip. Heating the ZIF-8-coated chip at 200 °C in air could regenerate the sensitivity and LSPR spectrum about a dozen times, although the degradation of ZIF-8 was revealed by the changes in the LSPR spectra, the XRD patterns, FT-IR spectra, and color of ZIF-8 after the gas treatments. In addition, the shift amount of the LSPR spectrum induced by humidity was much smaller than that of a DAPTMS-modified mesoporous-silica-coated chip. This will enable to measure the concentration of SO_2 and H_2S in volcanic gases using a humidity sensor to compensate for the effects of humidity without the use of a water absorbent or dehumidifier. Thus, the ZIF-8-coated chip demonstrated the high sensitivity, some selectivity and possibility of reuse under high humidity. These features are useful for periodic observation of SO_2 and H_2S in volcanic gases containing large amounts of H_2O. There is already a huge variety of MOFs, and new MOFs are still being developed. In future, more selective and robust MOFs of high adsorption capacity will improve sensor performances. Considering the enhancement of the sensitivity and selectivity by the amine-modified mesoporous silica, MOFs composed of organic linkers having amine groups will be promising candidates. Furthermore, multivariate analysis using multiple MOF-coated LSPR sensors will enable more accurate and practical detection of not only SO_2 and H_2S but also other volcanic gases.

As mentioned in Chapter 1, sensors such as electrochemical and semiconductor sensors can provide small and low-cost systems that have been used to observe volcanic gases remotely, safely, and in real time. Research on volcanic activity and disaster prevention will be advanced by overcoming the problems of sensors such as stability, cross-sensitivity, differences in response times. The LSPR sensor chips developed in this study could not solve such problems, but they showed the ability to detect SO_2 and H_2S in the target concentration range of 0.1 to 20 ppm. Based on the results of this study, the concept of the observation system using LSPR sensors is described as follows. The

system will be equipped with multiple LSPR sensors for various gas components in volcanic gases as shown in Figure 6.1. The area of the Au nanopattern in this study was 4 mm × 4 mm, but even a smaller area can be applied to measure the LSPR spectrum, facilitating the integration of LSPR sensors. For example, the system with 16 different sensors can be constructed by integrating the sensors with nanopattern areas of 1 mm × 1 mm coated with different adsorbents into an area of 4 mm × 4 mm. Light emitting diodes (LED) and photodiodes will be used as light sources and detectors. Band-pass filters may be used to adjust wavelength ranges appropriately. Thus, it is possible to build a system that is even smaller and cheaper than a system equipped with the same number of conventional sensors. Other components are a data logger and a battery, and by placing a water absorbent or dehumidifier at the inlet of the system, moisture can be removed from the volcanic gases. If the system is a hand-held size, it can be easily installed in many volcanoes. Its installation location will be slightly away from fumaroles as previous studies using electrochemical sensors. This is to avoid the risk of direct exposure to large amounts of water vapor and high concentrations of volcanic gases that are far beyond detection ranges of sensors.

Unlike conventional sensors, the sensors developed in this study did not show ON-OFF responses, but they have the potential to be used as sensors that accumulate concentrations of volcanic gases for a certain period. Such sensors cannot be used for real-time measurements of volcanic gases to track detailed temporal changes. However, they can be applied to periodic observations, such as five-minute measurements every hour. Periodic observations are still meaningful because current regular observations are also providing important data. In the future, real-time measurement will be possible by finding adsorbents and methods with good desorption performance that show ON-OFF responses. In addition, LSPR chips can be coated with a variety of adsorbents such as MOFs, enabling to detect any gases. Considering the results of this study, it will be difficult to make the LSPR sensors completely selective, but with many sensors and data analysis methods, it may be possible to detect all volcanic gas components that cannot be measured by the existing single observation system. Therefore, a small and inexpensive system equipped with multiple LSPR sensors can advance the study of volcanic activity.

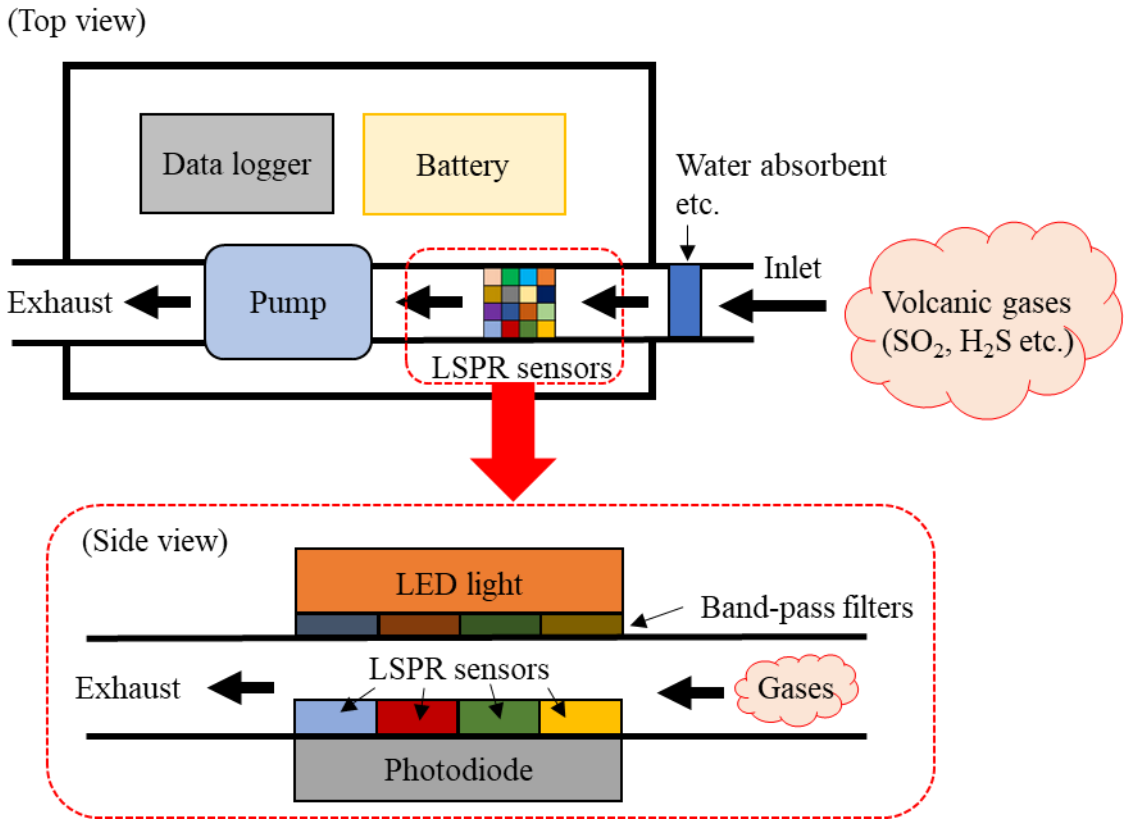

Figure 6.1. Schematic diagram of an observation system equipped with multiple LSPR sensors. The sensors of different colors are coated with different adsorbents.

Acknowledgements

I would like to express my sincere thanks to Professor Hiroyuki Kagi, The University of Tokyo, for his valuable suggestions, encouragement, generous guidance and supports throughout the course of this work.

I also would like to appreciate Associate Professor Toshiya Mori for his helpful advice, discussion, and encouragement.

I gratefully thank Professor Takafumi Hirata and Associate Professor Kazuki Komatsu for their beneficial suggestions and discussion.

I would like to express my gratitude to Professor Tetsuya Hasegawa, Professor Shunichi Nakai and Professor Takeaki Ozawa for the critical and valuable comments on this manuscript and discussion in my thesis defense.

I would like to show my gratitude to Professor Kazumasa Sugiyama, Tohoku University, for his fruitful suggestions, encouragement and providing me with samples.

I would like to express appreciation to Dr. Akira Monkawa, Tokyo Metropolitan Industrial Technology Research Institute, for giving me helpful suggestions, encouragement, and the opportunity to go to the Ph.D. course.

I am deeply grateful to my colleague Dr. Kohki Nagata for his valuable advice, discussion, and conduction of various experiments with me.

I would like to thank Dr. Elito Kazawa for teaching me the experimental techniques of NIL and providing me with Au-nanopatterned chips and Si molds fabricated by EBL.

I show my gratitude to Dr. Tomoko Gessei for her helpful advice, discussion, encouragement, and the preparation of samples.

I also thank Dr. Kazuo Morikawa and Dr. Daisuke Ogawa for SEM observations, and Ms. Mariko Kinoshita for adsorption-desorption measurements.

I am very thankful to Dr. Masahiro Kobayashi for his valuable advice, discussion, and encouragement.

I am also grateful to all staffs and members in the Geochemical Research Center, The University of Tokyo, for their various help, discussion, and motivation.

This work was financially supported by JSPS KAKENHI Grant Number 18K04789

(to Akira Monkawa).

Finally, I would like to express my deepest gratitude to my family for mentally supporting me during my Ph.D. course.

References

Ahmed, I., Jhung, S.H., 2016. Adsorptive desulfurization and denitrogenation using metal-organic frameworks. Journal of Hazard Mater 301, 259-276.

Aiuppa, A., Bertagnini, A., Métrich, N., Moretti, R., Di Muro, A., Liuzzo, M., Tamburello, G., 2010. A model of degassing for Stromboli volcano. Earth and Planetary Science Letters 295, 195-204.

Aiuppa, A., Burton, M., Allard, P., Caltabiano, T., Giudice, G., Gurrieri, S., Liuzzo, M., Salerno, G., 2011. First observational evidence for the CO_2-driven origin of Stromboli's major explosions. Solid Earth 2, 135-142.

Aiuppa, A., Federico, C., Giudice, G., Giuffrida, G., Guida, R., Gurrieri, S., Liuzzo, M., Moretti, R., Papale, P., 2009. The 2007 eruption of Stromboli volcano: Insights from real-time measurement of the volcanic gas plume CO_2/SO_2 ratio. Journal of Volcanology and Geothermal Research 182, 221-230.

Aiuppa, A., Federico, C., Giudice, G., Gurrieri, S., 2005. Chemical mapping of a fumarolic field: La Fossa Crater, Vulcano Island (Aeolian Islands, Italy). Geophysical Research Letters 32.

Aiuppa, A., Schmidt, A., Fristad, K.E., Elkins-Tanton, L.T., 2015. Volcanic-gas monitoring, Volcanism and Global Environmental Change, pp. 81-96.

Alayo, N., Conde-Rubio, A., Bausells, J., Borrise, X., Labarta, A., Batlle, X., Perez-Murano, F., 2015. Nanoparticles with tunable shape and composition fabricated by nanoimprint lithography. Nanotechnology 26, 445302.

Allan, P.K., Wheatley, P.S., Aldous, D., Mohideen, M.I., Tang, C., Hriljac, J.A., Megson, I.L., Chapman, K.W., De Weireld, G., Vaesen, S., Morris, R.E., 2012. Metal-organic frameworks for the storage and delivery of biologically active hydrogen sulfide. Dalton Transactions 41, 4060-4066.

Alothman, Z., 2012. A Review: Fundamental Aspects of Silicate Mesoporous Materials. Materials 5, 2874-2902.

Anker, J.N., Hall, W.P., Lyandres, O., Shah, N.C., Zhao, J., Van Duyne, R.P., 2008. Biosensing with plasmonic nanosensors. Nature Materials 7, 442.

Assen, A.H., Belmabkhout, Y., Adil, K., Bhatt, P.M., Xue, D.X., Jiang, H., Eddaoudi, M., 2015. Ultra-Tuning of the Rare-Earth fcu-MOF Aperture Size for Selective Molecular Exclusion of Branched Paraffins. Angewandte Chemie International Edition 54, 14353-14358.

Barbillon, G., Bijeon, J.L., Plain, J., de la Chapelle, M.L., Adam, P.M., Royer, P., 2007. Electron beam lithography designed chemical nanosensors based on localized surface plasmon resonance. Surface Science 601, 5057-5061.

Bezerra de Oliveira, H.J., Ferreira Martins Filho, J., do Nascimento, J.F., 2018. Computational Modeling of H_2S Gas Sensor Using Surface Plasmon Resonance in a D-Shaped Optical Fiber, 2018 SBFoton International Optics and Photonics Conference (SBFoton IOPC), pp. 1-5.

Bhattacharyya, S., Pang, S.H., Dutzer, M.R., Lively, R.P., Walton, K.S., Sholl, D.S., Nair, S., 2016. Interactions of SO_2-Containing Acid Gases with ZIF-8: Structural Changes and Mechanistic Investigations. The Journal of Physical Chemistry C 120, 27221-27229.

Bingham, J.M., Anker, J.N., Kreno, L.E., Van Duyne, R.P., 2010. Gas Sensing with High-Resolution Localized Surface Plasmon Resonance Spectroscopy. Journal of the American Chemical Society 132, 17358-17359.

Bluth, G.J.S., Shannon, J.M., Watson, I.M., Prata, A.J., Realmuto, V.J., 2007. Development of an ultra-violet digital camera for volcanic SO_2 imaging. Journal of Volcanology and Geothermal Research 161, 47-56.

Britt, D., Tranchemontagne, D., Yaghi, O.M., 2008. Metal-organic frameworks with high capacity and selectivity for harmful gases. Proceedings of the National Academy of Sciences 105, 11623–11627.

Cao, J., Sun, T., Grattan, K.T.V., 2014. Gold nanorod-based localized surface plasmon resonance biosensors: A review. Sensors and Actuators B: Chemical 195, 332-351.

Chang, Y.C., Chung, H.C., Lu, S.C., Guo, T.F., 2013. A large-scale sub-100 nm Au nanodisk array fabricated using nanospherical-lens lithography: a low-cost localized surface plasmon resonance sensor. Nanotechnology 24, 095302.

Chen, K.J., Lu, C.J., 2010. A vapor sensor array using multiple localized surface plasmon resonance bands in a single UV-vis spectrum. Talanta 81, 1670-1675.

Chen, R., Morris, H.R., Whitmore, P.M., 2013. Fast detection of hydrogen sulfide gas in the ppmv range with silver nanoparticle films at ambient conditions. Sensors and Actuators B: Chemical 186, 431-438.

Chen, Y., Xu, P., Xu, T., Zheng, D., Li, X., 2017. ZnO-nanowire size effect induced ultra-high sensing response to ppb-level H_2S. Sensors and Actuators B: Chemical 240, 264-272.

Chernikova, V., Yassine, O., Shekhah, O., Eddaoudi, M., Salama, Khaled N., 2018. Highly sensitive and selective SO_2 MOF sensor: the integration of MFM-300 MOF as a sensitive layer on a capacitive interdigitated electrode. Journal of Materials Chemistry A 6, 5550-5554.

Choi, M., Kim, N.-h., Eom, S., Kim, T.W., Byun, K.M., Park, H.-H., 2015. Fabrication and characterization of gold nanocrown arrays on a gold film for a high-sensitivity surface plasmon resonance biosensor. Thin Solid Films 587, 43-46.

Cittadini, M., Bersani, M., Perrozzi, F., Ottaviano, L., Wlodarski, W., Martucci, A., 2014. Graphene oxide coupled with gold nanoparticles for localized surface plasmon resonance based gas sensor. Carbon 69, 452-459.

Corma, A., García, H., Llabrés i Xamena, F.X., 2010. Engineering Metal Organic Frameworks for Heterogeneous Catalysis. Chemical Reviews 110, 4606–4655.

DeCoste, J.B., Peterson, G.W., 2014. Metal-organic frameworks for air purification of toxic chemicals. Chemical Reviews 114, 5695-5727.

Della Gaspera, E., Guglielmi, M., Agnoli, S., Granozzi, G., Post, M.L., Bello, V., Mattei, G., Martucci, A., 2010. Au Nanoparticles in Nanocrystalline TiO_2−NiO Films for SPR-Based, Selective H_2S Gas Sensing. Chemistry of Materials 22, 3407-3417.

Della Gaspera, E., Guglielmi, M., Perotto, G., Agnoli, S., Granozzi, G., Post, M.L., Martucci, A., 2012. CO optical sensing properties of nanocrystalline ZnO–Au films: Effect of doping with transition metal ions. Sensors and Actuators B: Chemical 161, 675-683.

Devito, S., Massera, E., Quercia, L., Difrancia, G., 2007. Analysis of volcanic gases by

means of electronic nose. Sensors and Actuators B: Chemical 127, 36-41.

Draine, B.T., Flatau, P.J., 1994. Discrete-Dipole Approximation For Scattering Calculations. Journal of the Optical Society of America A 11, 1491-1499.

Dutta, A., Tymińska, N., Zhu, G., Collins, J., Lively, R.P., Schmidt, J.R., Vasenkov, S., 2018. Influence of Hydrogen Sulfide Exposure on the Transport and Structural Properties of the Metal–Organic Framework ZIF-8. The Journal of Physical Chemistry C 122, 7278-7287.

Ethiraj, J., Bonino, F., Lamberti, C., Bordiga, S., 2015. H_2S interaction with HKUST-1 and ZIF-8 MOFs: A multitechnique study. Microporous and Mesoporous Materials 207, 90-94.

Francis, P., Chaffin, C., Maciejewski, A., Oppenheimer, C., 1996. Remote determination of SiF_4 in volcanic plumes: A new tool for volcano monitoring. Geophysical Research Letters 23, 249-252.

Fukuhara, M., Ono, H., Hirasawa, T., Otaguchi, M., Sakai, N., Mizuno, J., Shoji, S., 2007. UV Nanoimprint Lithography and Its Application for Nanodevices. Journal of Photopolymer Science and Technology 20, 549-554.

Furukawa, H., Cordova, K.E., O'Keeffe, M., Yaghi, O.M., 2013. The chemistry and applications of metal-organic frameworks. Science 341, 1230444.

Georgiadis, A., Charisiou, N., Goula, M., 2020. Removal of Hydrogen Sulfide From Various Industrial Gases: A Review of The Most Promising Adsorbing Materials. Catalysts 10.

Giggenbach, W.F., 1975. A Simple Method for the Collection and Analysis of Volcanic Gas Samples. Bulletin Volcanologique volume 39, 132–145.

Gliemann, H., Wöll, C., 2012. Epitaxially grown metal-organic frameworks. Materials Today 15, 110-116.

Gong, X., Wang, Y., Kuang, T., 2017. ZIF-8-Based Membranes for Carbon Dioxide Capture and Separation. ACS Sustainable Chemistry & Engineering 5, 11204-11214.

Grant Glover, T., Peterson, G.W., Schindler, B.J., Britt, D., Yaghi, O., 2011. MOF-74 building unit has a direct impact on toxic gas adsorption. Chemical Engineering

Science 66, 163-170.

Haes, A.J., Haynes, C.L., McFarland, A.D., Schatz, G.C., Van Duyne, R.P., Zou, S., 2005. Plasmonic Materials for Surface-Enhanced Sensing and Spectroscopy. MRS Bulletin 30, 368-375.

Hamon, L., Serre, C., Devic, T., Loiseau, T., Millange, F., Fe´rey, G.r., Weireld, G.D., 2009. Comparative Study of Hydrogen Sulfide Adsorption in the MIL-53(Al, Cr, Fe), MIL-47(V), MIL-100(Cr), and MIL-101(Cr) Metal-Organic Frameworks at Room Temperature. Journal of the American Chemical Society 131, 8775–8777.

Haynes, C.L., Duyne, R.P.V., 2001. Nanosphere Lithography: A Versatile Nanofabrication Tool for Studies of Size-Dependent Nanoparticle Optics. The Journal of Physical Chemistry B 105, 5599-5611.

Hicks, E.M., Zou, S., Schatz, G.C., Spears, K.G., Duyne, R.P.V., 2005. Controlling Plasmon Line Shapes through Diffractive Coupling in Linear Arrays of Cylindrical Nanoparticles Fabricated by Electron Beam Lithography. NAno Letters 5, 1065-1070.

Hirabayashi, J., 1986. Present status of researches on disasters caused by volcanic gases and prediction of volcanic eruption by chemical methods. Kazan. Dai 2 shu (Volcanoes. Vol. 2) 30, S327-S338. (In Japanese with English abstract)

Hirabayashi, J., 2015. Volcanic gases. Chishitsukogaku (Geotechnology) 13, 16-22. (In Japanese)

Hong, E., Kim, J.H., 2014. Oxide content optimized ZnS–ZnO heterostructures via facile thermal treatment process for enhanced photocatalytic hydrogen production. International Journal of Hydrogen Energy 39, 9985-9993.

Hosseini, Z.S., Mortezaali, A., Iraji zad, A., Fardindoost, S., 2015. Sensitive and selective room temperature H2S gas sensor based on Au sensitized vertical ZnO nanorods with flower-like structures. Journal of Alloys and Compounds 628, 222-229.

Hozumi, A., Yokogawa, Y., Kameyama, T., Sugimura, H., Hayashi, K., Shirayama, H., Takai, O., 2001. Amino-terminated self-assembled monolayer on a SiO_2 surface formed by chemical vapor deposition. Journal of Vacuum Science & Technology A: Vacuum, Surfaces, and Films 19, 1812-1816.

Iguchi, M., Nakamichi, H., Tameguri, T., Yamamoto, K., Mori, T., Ohminato, T., Saito, E., 2017. Contribution of monitoring data to decision making for evacuation from the 2014 and 2015 eruptions of Kuchinoerabujima Volcano. Journal of Natural Disaster Science 38, 31-47.

Jo, N.R., Lee, K.J., Shin, Y.B., 2016. Enzyme-coupled nanoplasmonic biosensing of cancer markers in human serum. Biosensors and Bioelectronics 81, 324-333.

Joy, N.A., Nandasiri, M.I., Rogers, P.H., Jiang, W., Varga, T., Kuchibhatla, S.V., Thevuthasan, S., Carpenter, M.A., 2012. Selective plasmonic gas sensing: H_2, NO_2, and CO spectral discrimination by a single Au-CeO_2 nanocomposite film. Analytical Chemistry 84, 5025-5034.

Kang, M., Losego, M., Sachet, E., Maria, J.-P., Franzen, S., 2016. Near-Infrared Optical Extinction of Indium Tin Oxide Structures Prepared by Nanosphere Lithography. ACS Photonics 3, 1993-1999.

Khabazipour, M., Anbia, M., 2019. Removal of Hydrogen Sulfide from Gas Streams Using Porous Materials: A Review. Industrial & Engineering Chemistry Research 58, 22133-22164.

Kreno, L.E., Hupp, J.T., Van Duyne, R.P., 2010. Metal−Organic Framework Thin Film for Enhanced Localized Surface Plasmon Resonance Gas Sensing. Analytical Chemistry 82, 8042-8046.

Kreno, L.E., Leong, K., Farha, O.K., Allendorf, M., Van Duyne, R.P., Hupp, J.T., 2012. Metal-organic framework materials as chemical sensors. Chemical Reviews 112, 1105-1125.

Kusakabe, M., Ohsumi, T., 1987. Outburst of carbon dioxide from Lake Nyos, Cameroon. Chikyukagaku (Geochemistry) 21, 39-47. (In Japanese with English abstract)

Le Guern, F., Tazieff, H., Pierret, R.F., 1982. An example of health hazard: People killed by gas during a phreatic eruption: Diëng plateau (Java, Indonesia), February 20th 1979. Bulletin Volcanologique 45, 153-156.

Lee, J., Lee, K., Kim, J., 2021. Fiber-Based Gas Filter Assembled via In Situ Synthesis of ZIF-8 Metal Organic Frameworks for an Optimal Adsorption of SO_2: Experimental and Theoretical Approaches. ACS Applied Materials & Interfaces

13, 1620-1631.

Li, H., Wang, K., Sun, Y., Lollar, C.T., Li, J., Zhou, H.-C., 2018. Recent advances in gas storage and separation using metal–organic frameworks. Materials Today 21, 108-121.

Li, L., Sun, T.H., Shu, C.H., Zhang, H.B., 2016. Low temperature H_2S removal with 3-D structural mesoporous molecular sieves supported ZnO from gas stream. Journal of Hazardous Materials 311, 142-150.

Liang, K., Ricco, R., Doherty, C.M., Styles, M.J., Bell, S., Kirby, N., Mudie, S., Haylock, D., Hill, A.J., Doonan, C.J., Falcaro, P., 2015. Biomimetic mineralization of metal-organic frameworks as protective coatings for biomacromolecules. Nature Communications 6, 7240.

Lin, P.Y., Le, G.Y., Chiu, W.I., Jian, R.S., Lu, C.J., 2019. A single light spot GC detector employing localized surface plasmon resonance of porous Au@SiO_2 nanoparticle multilayer. Analyst 144, 698-706.

Lin, Y., Zou, Y., Mo, Y., Guo, J., Lindquist, R.G., 2010. E-beam patterned gold nanodot arrays on optical fiber tips for localized surface plasmon resonance biochemical sensing. Sensors 10, 9397-9406.

Liu, J., Wei, Y., Li, P., Zhao, Y., Zou, R., 2017. Selective H_2S/CO_2 Separation by Metal–Organic Frameworks Based on Chemical-Physical Adsorption. The Journal of Physical Chemistry C 121, 13249-13255.

Liu, Z., 2017. One-step fabrication of crystalline metal nanostructures by direct nanoimprinting below melting temperatures. Nature Communications 8, 14910.

Lu, G., Hupp, J.T., 2010. Metal-Organic Frameworks as Sensors: A ZIF-8 Based Fabry-Pe´rot Device as a Selective Sensor for Chemical Vapors and Gases. Journal of the American Chemical Society 132, 7832–7833.

Lupan, O., Chow, L., Chai, G., 2009. A single ZnO tetrapod-based sensor. Sensors and Actuators B: Chemical 141, 511-517.

Marcu, I.-C., Sandulescu, I., 2004. Study of sulfur dioxide adsorption on Y zeolite. Journal of the Serbian Chemical Society 69, 563–569.

Martínez-Ahumada, E., López-Olvera, A., Jancik, V., Sánchez-Bautista, J.E., González-

Zamora, E., Martis, V., Williams, D.R., Ibarra, I.A., 2020. MOF Materials for the Capture of Highly Toxic H_2S and SO_2. Organometallics 39, 883-915.

McGonigle, A.J.S., Aiuppa, A., Giudice, G., Tamburello, G., Hodson, A.J., Gurrieri, S., 2008. Unmanned aerial vehicle measurements of volcanic carbon dioxide fluxes. Geophysical Research Letters 35.

Mekaru, H., 2014. Formation of metal nanostructures by high-temperature imprinting. Microsystem Technologies 20, 1103-1109.

Mishra, S.K., Rani, S., Gupta, B.D., 2014. Surface plasmon resonance based fiber optic hydrogen sulphide gas sensor utilizing nickel oxide doped ITO thin film. Sensors and Actuators B: Chemical 195, 215-222.

Monkawa, A., Nakagawa, T., Sugimori, H., Kazawa, E., Sibamoto, K., Takei, T., Haruta, M., 2014. With high sensitivity and with wide-dynamic-range localized surface-plasmon resonance sensor for volatile organic compounds. Sensors and Actuators B: Chemical 196, 1-9.

Mori, T., Hashimoto, T., Terada, A., Yoshimoto, M., Kazahaya, R., Shinohara, H., Tanaka, R., 2016. Volcanic plume measurements using a UAV for the 2014 Mt. Ontake eruption. Earth, Planets and Space 68.

Mori, T., Ishihara, K., Hirabayashi, J., Kazahaya, K., Mori, T., 2004. SO_2 gas monitoring by DOAS at Sakurajima and Suwanosejima volcanoes. Annuals of Disaster Prevention Research Institute, Kyoto University 47, 157-162.

Mori, T., Notsu, K., 1997. Remote CO, COS, CO_2, SO_2, HCl detection and temperature estimation of volcanic gas. Geophysical Research Letters 24, 2047-2050.

Mori, T., Notsu, K., 2008. Temporal variation in chemical composition of the volcanic plume from Aso volcano, Japan, measured by remote FT-IR spectroscopy. Geochemical Journal 42, 133-140.

Mori, T., Notsu, K., Tohjima, Y., Wakita, H., 1993. Remote detection of HCl and SO_2 in volcanic gas from Unzen Volcano, Japan. Geophysical Research Letters 20, 1355-1358.

Nakagawa, S., 1966. Wet detoxification, recovery, and utilization of sulfurous acid gas in exhaust gas. Bunsekikagaku (Analytical chemistry) 15, 872-881. (In Japanese)

Notsu, K., Mori, T., Igarashi, G., Tohjima, Y., Wakita, H., 1993. Infrared spectral radiometer: A new tool for remote measurement of SO_2 of volcanic gas. Geochemical Journal 27, 361-366.

Okonkwo, C.N., Okolie, C., Sujan, A., Zhu, G., Jones, C.W., 2018. Role of Amine Structure on Hydrogen Sulfide Capture from Dilute Gas Streams Using Solid Adsorbents. Energy & Fuels 32, 6926-6933.

Omidi, M., Amoabediny, G., Yazdian, F., Habibi-Rezaei, M., 2015. Protein-based nanobiosensor for direct detection of hydrogen sulfide. EPL (Europhysics Letters) 109.

Oppenheimer, C., Francis, P., Burton, M., Maciejewski, A.J.H., Boardman, L., 1998. Remote measurement ofvolcanic gases by Fourier transform infrared spectroscopy. Applied Physics B Lasers and Optics 67, 505–515.

Oppenheimer, C., Scaillet, B., Martin, R.S., 2011. Sulfur Degassing From Volcanoes: Source Conditions, Surveillance, Plume Chemistry and Earth System Impacts. Reviews in Mineralogy and Geochemistry, Mineralogical Society 73, 363-421.

Oppenheimera, C., Burtonb, M.R., Durieuxc, J., Pyle, D.M., 2002. Open-path Fourier transform spectroscopy of gas emissions from Oldoinyo Lengai volcano, Tanzania. Optics and Lasers in Engineering 37, 203–214.

Oskooi, A.F., Roundy, D., Ibanescu, M., Bermel, P., Joannopoulos, J.D., Johnson, S.G., 2010. Meep: A flexible free-software package for electromagnetic simulations by the FDTD method. Computer Physics Communications 181, 687-702.

Özgür, Ü., Alivov, Y.I., Liu, C., Teke, A., Reshchikov, M.A., Doğan, S., Avrutin, V., Cho, S.J., Morkoç, H., 2005. A comprehensive review of ZnO materials and devices. Journal of Applied Physics 98.

Özgür, Ü., Hofstetter, D., Morkoç, H., 2010. ZnO Devices and Applications: A Review of Current Status and Future Prospects. Proceedings of the IEEE 98, 1255-1268.

Pan, Y., Liu, Y., Zeng, G., Zhao, L., Lai, Z., 2011. Rapid synthesis of zeolitic imidazolate framework-8 (ZIF-8) nanocrystals in an aqueous system. Chemical Communications 47, 2071-2073.

Pang, S.H., Han, C., Sholl, D.S., Jones, C.W., Lively, R.P., 2016. Facet-Specific Stability

of ZIF-8 in the Presence of Acid Gases Dissolved in Aqueous Solutions. Chemistry of Materials 28, 6960-6967.

Park, K.S., Ni, Z., Côté, A.P., Choi, J.Y., Huang, R., Uribe-Romo, F.J., Chae, H.K., O'Keeffe, M., Yaghi, O.M., 2006. Exceptional chemical and thermal stability of zeolitic imidazolate frameworks. Proceedings of the National Academy of Sciences 103, 10186-10191.

Pellas, V., Hu, D., Mazouzi, Y., Mimoun, Y., Blanchard, J., Guibert, C., Salmain, M., Boujday, S., 2020. Gold Nanorods for LSPR Biosensing: Synthesis, Coating by Silica, and Bioanalytical Applications. Biosensors 10.

Rackauskas, S., Barbero, N., Barolo, C., Viscardi, G., 2017. ZnO Nanowire Application in Chemoresistive Sensing: A Review. Nanomaterials 7.

Reiffenstein, R.J., Hulbert, W.C., Roth, S.H., 1992. Toxicology of Hydrogen Sulfide. Annual Review of Pharmacology and Toxicology 32, 109-134.

Rezaei, F., Rownaghi, A.A., Monjezi, S., Lively, R.P., Jones, C.W., 2015. SO_x/NO_x Removal from Flue Gas Streams by Solid Adsorbents: A Review of Current Challenges and Future Directions. Energy & Fuels 29, 5467-5486.

Roberts, T.J., Braban, C.F., Oppenheimer, C., Martin, R.S., Freshwater, R.A., Dawson, D.H., Griffiths, P.T., Cox, R.A., Saffell, J.R., Jones, R.L., 2012. Electrochemical sensing of volcanic gases. Chemical Geology 332-333, 74-91.

Roberts, T.J., Lurton, T., Giudice, G., Liuzzo, M., Aiuppa, A., Coltelli, M., Vignelles, D., Salerno, G., Coute, B., Chartier, M., Baron, R., Saffell, J.R., Scaillet, B., 2017. Validation of a novel Multi-Gas sensor for volcanic HCl alongside H_2S and SO_2 at Mt. Etna. Bulletin of Volcanology 79, 36.

Roberts, T.J., Saffell, J.R., Oppenheimer, C., Lurton, T., 2014. Electrochemical sensors applied to pollution monitoring: Measurement error and gas ratio bias — A volcano plume case study. Journal of Volcanology and Geothermal Research 281, 85-96.

Sakai, N., 2009. Photo-curable Resin for UV-Nanoimprint Technology. Journal of Photopolymer Science and Technology 22, 133-145.

Sánchez-Sánchez, M., Getachew, N., Díaz, K., Díaz-García, M., Chebude, Y., Díaz, I.,

2015. Synthesis of metal–organic frameworks in water at room temperature: salts as linker sources. Green Chemistry 17, 1500-1509.

Savage, M., Cheng, Y., Easun, T.L., Eyley, J.E., Argent, S.P., Warren, M.R., Lewis, W., Murray, C., Tang, C.C., Frogley, M.D., Cinque, G., Sun, J., Rudic, S., Murden, R.T., Benham, M.J., Fitch, A.N., Blake, A.J., Ramirez-Cuesta, A.J., Yang, S., Schroder, M., 2016. Selective Adsorption of Sulfur Dioxide in a Robust Metal-Organic Framework Material. Advanced Materials 28, 8705-8711.

Shah, M.S., Tsapatsis, M., Siepmann, J.I., 2017. Hydrogen Sulfide Capture: From Absorption in Polar Liquids to Oxide, Zeolite, and Metal-Organic Framework Adsorbents and Membranes. Chemical Reviews 117, 9755-9803.

Shanmugam, N.R., Muthukumar, S., Prasad, S., 2017. A review on ZnO-based electrical biosensors for cardiac biomarker detection. Future Science OA 3.

Shimoike, Y., Notsu, K., 2000. Continuous chemical monitoring of volcanic gas in Izu-Oshima volcano, Japan. Journal of Volcanology and Geothermal Research 101, 211–221.

Shinde, S.D., Patil, G.E., Kajale, D.D., Gaikwad, V.B., Jain, G.H., 2012. Synthesis of ZnO nanorods by spray pyrolysis for H_2S gas sensor. Journal of Alloys and Compounds 528, 109-114.

Shinohara, H., 2005a. The Present and Future of Volcanic Gas Monitoring for Forecasting Volcanic Eruptions. Kazan (Volcanoes) 50, S167-S176. (In Japanese with English abstract)

Shinohara, H., 2005b. A new technique to estimate volcanic gas composition: plume measurements with a portable multi-sensor system. Journal of Volcanology and Geothermal Research 143, 319-333.

Shinohara, H., 2013. Composition of volcanic gases emitted during repeating Vulcanian eruption stage of Shinmoedake, Kirishima volcano, Japan. Earth, Planets and Space 65, 667-675.

Shinohara, H., Matsushima, N., Kazahaya, K., Ohwada, M., 2011. Magma-hydrothermal system interaction inferred from volcanic gas measurements obtained during 2003–2008 at Meakandake volcano, Hokkaido, Japan. Bulletin of Volcanology

73, 409-421.

Shinohara, H., 2019. Processes Controlling Evolution of Volcanic Activity Deduced from Volcanic Gas Observations. Kazan (Volcanoes) 64, 121-129. (In Japanese with English abstract)

Small, L.J., Nenoff, T.M., 2017. Direct Electrical Detection of Iodine Gas by a Novel Metal-Organic-Framework-Based Sensor. ACS Applied Materials & Interfaces 9, 44649-44655.

Song, L., Zhang, L., Huang, Y., Chen, L., Zhang, G., Shen, Z., Zhang, J., Xiao, Z., Chen, T., 2017. Amplifying the signal of localized surface plasmon resonance sensing for the sensitive detection of Escherichia coli O157:H7. Scientific Reports 7, 3288.

Stoiber, R.E., Jepsen, A., 1973. Sulfur Dioxide Contributions to the Atmosphere by Volcanoes. Science 182, 577-578.

Sturaro, M., Della Gaspera, E., Cantalini, C., Guglielmi, M., Martucci, A., 2017. Near Infrared Plasmonic Gas Sensing with Doped Metal Oxide Nanocrystals. Proceedings 1.

Sun, Y., Zhou, H.C., 2015. Recent progress in the synthesis of metal-organic frameworks. Science and Technology of Advanced Materials 16, 054202.

Tabassum, R., Mishra, S.K., Gupta, B.D., 2013. Surface plasmon resonance-based fiber optic hydrogen sulphide gas sensor utilizing Cu-ZnO thin films. Physical Chemistry Chemical Physics 15, 11868-11874.

Tabassum, S., Kumar, R., Dong, L., 2017. Plasmonic Crystal-Based Gas Sensor Toward an Optical Nose Design. IEEE Sensors Journal 17, 6210-6223.

Tailor, R., Ahmadalinezhad, A., Sayari, A., 2014. Selective removal of SO_2 over tertiary amine-containing materials. Chemical Engineering Journal 240, 462-468.

Tailor, R., Sayari, A., 2016. Grafted propyldiethanolamine for selective removal of SO_2 in the presence of CO_2. Chemical Engineering Journal 289, 142-149.

Tan, K., Canepa, P., Gong, Q., Liu, J., Johnson, D.H., Dyevoich, A., Thallapally, P.K., Thonhauser, T., Li, J., Chabal, Y.J., 2013. Mechanism of Preferential Adsorption of SO_2 into Two Microporous Paddle Wheel Frameworks $M(bdc)(ted)_{0.5}$. Chemistry of Materials 25, 4653-4662.

Tran, U.P.N., Le, K.K.A., Phan, N.T.S., 2011. Expanding Applications of Metal−Organic Frameworks: Zeolite Imidazolate Framework ZIF-8 as an Efficient Heterogeneous Catalyst for the Knoevenagel Reaction. ACS Catalysis 1, 120-127.

Usha, S.P., Mishra, S.K., Gupta, B.D., 2015. Fiber optic hydrogen sulfide gas sensors utilizing ZnO thin film/ZnO nanoparticles: A comparison of surface plasmon resonance and lossy mode resonance. Sensors and Actuators B: Chemical 218, 196-204.

Vikrant, K., Kumar, V., Ok, Y.S., Kim, K.-H., Deep, A., 2018. Metal-organic framework (MOF)-based advanced sensing platforms for the detection of hydrogen sulfide. Trends in Analytical Chemistry 105, 263-281.

Wan, Q., Lin, C.L., Yu, X.B., Wang, T.H., 2004. Room-temperature hydrogen storage characteristics of ZnO nanowires. Applied Physics Letters 84, 124-126.

Wang, C., Chu, X., Wu, M., 2006. Detection of H_2S down to ppb levels at room temperature using sensors based on ZnO nanorods. Sensors and Actuators B: Chemical 113, 320-323.

Wang, J., Chen, R., Xiang, L., Komarneni, S., 2018. Synthesis, properties and applications of ZnO nanomaterials with oxygen vacancies: A review. Ceramics International 44, 7357-7377.

Wang, L., Xiong, W., Nishijima, Y., Misawa, H., Yokota, Y., Qiu, J., Ueno, K., Bi, G., 2011. Spectral properties of nanoengineered Ag/Au bilayer rods fabricated by electron beam lithography. Applied Optics 50, 5600-5605.

Wang, X., Ma, X., Sun, L., Song, C., 2007. A nanoporous polymeric sorbent for deep removal of H_2S from gas mixtures for hydrogen purification. Green Chemistry 9.

Weibringa, P., Swartlinga, J., Ednera, H., Svanberga, S., Caltabianob, T., Condarellib, D., Cecchic, G., Pantani, L., 2002. Optical monitoring of volcanic sulphur dioxide emissionsFcomparison between four different remote-sensing spectroscopic techniques. Optics and Lasers in Engineering 37, 267–284.

Wetchakun, K., Samerjai, T., Tamaekong, N., Liewhiran, C., Siriwong, C., Kruefu, V., Wisitsoraat, A., Tuantranont, A., Phanichphant, S., 2011. Semiconducting metal oxides as sensors for environmentally hazardous gases. Sensors and Actuators B:

Chemical 160, 580-591.

Wiheeb, A.D., Shamsudin, I.K., Ahmad, M.A., Murat, M.N., Kim, J., Othman, M.R., 2013. Present technologies for hydrogen sulfide removal from gaseous mixtures. Reviews in Chemical Engineering 29.

Willets, K.A., Van Duyne, R.P., 2007. Localized surface plasmon resonance spectroscopy and sensing. Annual Review of Physical Chemistry 58, 267-297.

Witt, M.L.I., Fischer, T.P., Pyle, D.M., Yang, T.F., Zellmer, G.F., 2008. Fumarole compositions and mercury emissions from the Tatun Volcanic Field, Taiwan: Results from multi-component gas analyser, portable mercury spectrometer and direct sampling techniques. Journal of Volcanology and Geothermal Research 178, 636-643.

Wong, M.W., Wiberg, K.B., 1992. Structures, bonding, and absorption spectra of amine-sulfur dioxide charge-transfer complexes. Journal of the American Chemical Society 114, 7527–7535.

Wu, C., Xu, Q.H., 2009. Stable and functionable mesoporous silica-coated gold nanorods as sensitive localized surface plasmon resonance (LSPR) nanosensors. Langmuir 25, 9441-9446.

Yamada, T., Ueda, H., Mori, T., Tanada, T., 2019. Tracing Volcanic Activity Chronology from a Multiparameter Dataset at Shinmoedake Volcano (Kirishima), Japan. Journal of Disaster Research 14, 687-700.

Yang, S., Sun, J., Ramirez-Cuesta, A.J., Callear, S.K., David, W.I., Anderson, D.P., Newby, R., Blake, A.J., Parker, J.E., Tang, C.C., Schroder, M., 2012. Selectivity and direct visualization of carbon dioxide and sulfur dioxide in a decorated porous host. Nature Chemistry 4, 887-894.

Yang, S.C., Hou, J.L., Finn, A., Kumar, A., Ge, Y., Fischer, W.J., 2015. Synthesis of multifunctional plasmonic nanopillar array using soft thermal nanoimprint lithography for highly sensitive refractive index sensing. Nanoscale 7, 5760-5766.

Yassine, O., Shekhah, O., Assen, A.H., Belmabkhout, Y., Salama, K.N., Eddaoudi, M., 2016. H_2S Sensors: Fumarate-Based fcu-MOF Thin Film Grown on a Capacitive Interdigitated Electrode. Angewandte Chemie International Edition 55, 15879-

15883.

Yu, C.-C., Chen, H.-L., 2015. Nanoimprint technology for patterning functional materials and its applications. Microelectronic Engineering 132, 98-119.

Yurkin, M.A., Hoekstra, A.G., Brock, R.S., Lu, J.Q., 2007. Systematic comparison of the discrete dipole approximation and the finite difference time domain method for large dielectric scatterers. Optics Express 15, 17902-17911.

Zhang, W., Wang, C., Zhou, W., Yue, Z., Liu, G.H., 2011. The Analysis of Ag Nanospheres and Arrays LSPR Phenomena Based on DDA and FDTD Method. Applied Mechanics and Materials 110-116, 3860-3866.

Zhao, D., Huo, Q., Feng, J., Chmelka, B.F., Stucky, G.D., 1998. Nonionic Triblock and Star Diblock Copolymer and Oligomeric Surfactant Syntheses of Highly Ordered, Hydrothermally Stable, Mesoporous Silica Structures. Journal of the American Chemical Society 120, 6024-6036.

Zhi, Y., Zhou, Y., Su, W., Sun, Y., Zhou, L., 2011. Selective Adsorption of SO_2 from Flue Gas on Triethanolamine-Modified Large Pore SBA-15. Industrial & Engineering Chemistry Research 50, 8698-8702.

Zou, W., Liu, W., Luo, L., Zhang, S., Lu, R., Veser, G., 2012. Detection of nitro explosives via LSPR sensitive silver clusters embedded in porous silica. Journal of Materials Chemistry 22.